REPORT DOCUMENTATION PAGE

Form Approved
OMB NO. 0704-0188

1. AGENCY USE ONLY (Leave Blank)

2. REPORT DATE 5-3-01

3. REPORT TYPE AND DATES COVERED
Final Report 01 Jun 96 - 31 May 00

4. TITLE AND SUBTITLE

Elastomeric Nanocomposites Based on Sol-Gel Reactions of Silicon Alkoxides in Ionomeric Derivatives of Finely-Architectured Block Copolymers

5. FUNDING NUMBERS
DAAH04-96-1-0191

6. AUTHOR(S)

Kenneth A. Mauritz and Robson F. Storey

7. PERFORMING ORGANIZATION NAME(S) AND ADDRESS(ES)

University of So. MS
Dept. Of Polymer Science
Box 10076
Hattiesburg, MS 39406-0076

8. PERFORMING ORGANIZATION REPORT NUMBER

9. SPONSORING / MONITORING AGENCY NAME(S) AND ADDRESS(ES)

U. S. Army Research Office
P.O. Box 12211
Research Triangle Park, NC 27709-2211

10. SPONSORING / MONITORING AGENCY REPORT NUMBER

35826-CH-DPS
.1

11. SUPPLEMENTARY NOTES

The views, opinions and/or findings contained in this report are those of the author(s) and should not be construed as an official Department of the Army position, policy or decision, unless so designated by other documentation.

12 a. DISTRIBUTION / AVAILABILITY STATEMENT

Approved for public release; distribution unlimited.

12 b. DISTRIBUTION CODE

13. ABSTRACT (Maximum 200 words)

The goal of the proposed research is lightweight elastomers to be used in clothing that protects soldiers from chemical warfare agents (CWAs). Outward transport of water from perspiration is another important requirement. Our approach addresses the simultaneous fulfillment of these requirements through the manipulation of the heterogeneous architecture, followed by the inorganic modification of hard/soft block copolymer (BCP) elastomers. An inorganic component is inserted within the sulfonated hard block domains in block copolymer ionomers (BCPIs) via *in situ* sol-gel reactions for hydrolyzed silicon alkoxides.

14. SUBJECT TERMS

15. NUMBER OF PAGES
44

16. PRICE CODE

17. SECURITY CLASSIFICATION OR REPORT	18. SECURITY CLASSIFICATION ON THIS PAGE	19. SECURITY CLASSIFICATION OF ABSTRACT	20. LIMITATION OF ABSTRACT
UNCLASSIFIED	UNCLASSIFIED	UNCLASSIFIED	UL

NSN 7540-01-280-5500

Standard Form 298 (Rev.2-89)
Prescribed by ANSI Std. 239-18
298-102

Enclosure 1

Enclosure 2

MASTER COPY: PLEASE KEEP THIS "MEMORANDUM OF TRANSMITTAL" BLANK FOR REPRODUCTION PURPOSES. WHEN REPORTS ARE GENERATED UNDER THE ARO SPONSORSHIP, FORWARD A COMPLETED COPY OF THIS FORM WITH EACH REPORT SHIPMENT TO THE ARO. THIS WILL ASSURE PROPER IDENTIFICATION. NOT TO BE USED FOR INTERIM PROGRESS REPORTS; SEE PAGE 2 FOR INTERIM PROGRESS REPORT INSTRUCTIONS.

MEMORANDUM OF TRANSMITTAL

U.S. Army Research Office
ATTN: AMSRL-RO-BI (TR)
P.O. Box 12211
Research Triangle Park, NC 27709-2211

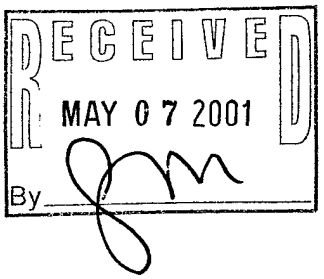

☐ Reprint (Orig + 2 copies)

☐ Technical Report (Orig + 2 copies)

☐ Manuscript (1 copy)

☒ Final Progress Report (Orig + 2 copies)

☐ Related Materials, Abstracts, Theses (1 copy)

CONTRACT/GRANT NUMBER: DAAH04-96-1-0191

REPORT TITLE: Elastomeric Nanocomposites Based on Sol-Gel Reactions of Silicon Alkoxides in Ionomeric Derivatives of Finely-Architectured Block Copolymers

is forwarded for your information.

SUBMITTED FOR PUBLICATION TO (applicable only if report is manuscript):

Sincerely,

Kenneth Mauritz and Robson Storey

I. GENERAL INTRODUCTION

The ultimate goal of this research, in terms of a U.S. Army mission, is to produce lightweight, mechanically durable, elastomeric materials with selective gas transport properties that can be used in clothing that protects military personnel from chemical warfare agents (CWAs). The outward transport of water through this clothing owing to perspiration is another practical requirement. We have made progress with regard to this latter issue in this reporting period. Our hypothesis is that the simultaneous fulfillment of these requirements is possible through the manipulation of the heterogeneous architecture, followed by the inorganic modification of hard/soft block copolymer (BCP) elastomers. One variant of this approach consists of inserting an inorganic component within sulfonated hard block domains in block copolymer ionomers (BCPIs) via *in situ* sol-gel reactions for hydrolyzed silicon alkoxides.

The hard and soft blocks of interest are polystyrene (PS) and polyisobutylene (PIB), respectively, due in large part to the proven superior barrier properties of PIB. The precursor poly(styrene-*b*-isobutylene-*b*-styrene) (PS-PIB-PS) block copolymer elastomers, and sulfonated ionomers derived therefrom, are prepared using controlled/living carbocationic polymerization. Figure 1-I shows various architectures currently being explored including linear triblock and multi-arm star-block copolymers (**L-1**, **T-1**, and **S-1**). Unique telechelic polyisobutylenes possessing silicon alkoxide functional groups at chain termini (**L-2** and **T-2**) and BCPs possessing such groups at the block junctions (**L-3** and **T-3**) are also targeted. The latter will promote the formation of covalent linkages between organic and inorganic phases.

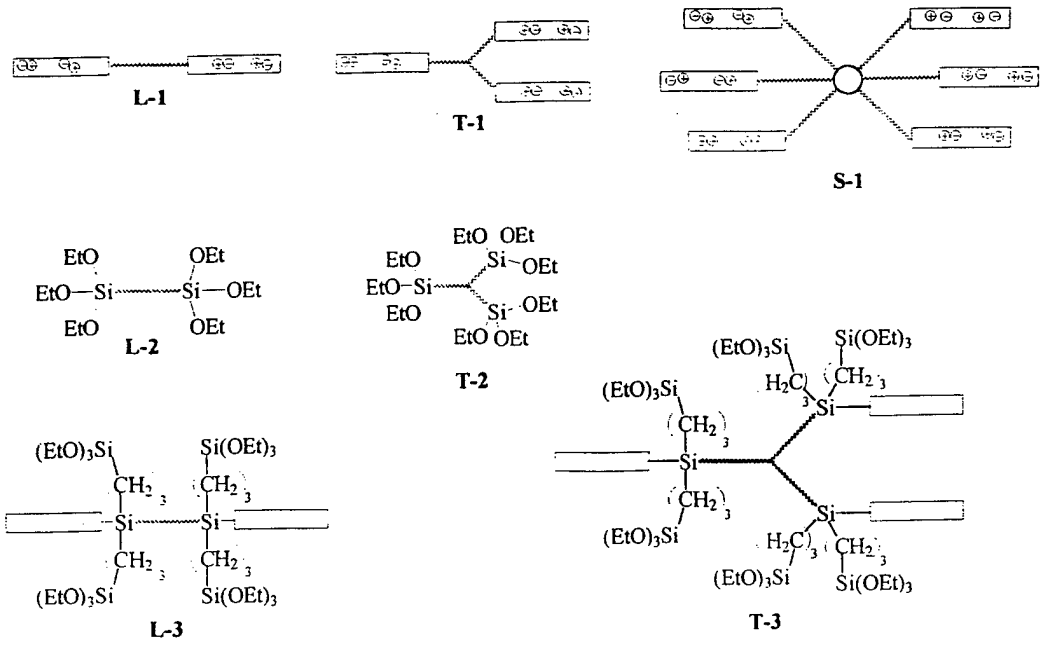

Figure 1-I. Various PIB-based elastomeric matrix polymers.

Sulfonated BCPIs serve the role of *morphological templates* that direct *in situ* sol-gel reactions for silicon alkoxides with the goal of creating elastomeric organic-inorganic hybrid materials with specific diffusion properties. These heterogeneous materials can be said to be "self-assembled" in two different stages. In order to incorporate inorganic phases via *in situ* sol-gel processes, solvents must be found that swell the BCPI to facilitate migration of hydrolyzed $Si(OR)_4$ monomers to ionic groups in the hard block domains - and do not degrade the BCPI matrix in the process. Part of our effort was concentrated on this activity. Hydrolyzed tetraethylorthosilicate (TEOS) molecules undergo consecutive condensation reactions, $Si(OH)_4 + Si(OH)_4 \rightarrow (HO)_3Si\text{-}O\text{-}Si(OH)_3 + H_2O$, so that silicate nanoparticles ultimately reside about these ionic sites after drying, as crudely illustrated in Figure 2-I.

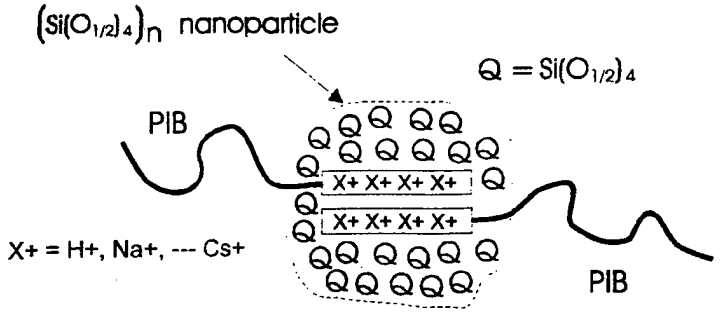

Figure 2-I. Silicate growth about an association of two ion-functionalized hard blocks. Actual hard domains will contain considerably more blocks.

As seen in our earlier efforts to create [organic polymer]/silicate hybrid materials, a large population of SiOH groups can be made to reside at the "surfaces" of these nanoparticles, particularly if the sol-gel reaction is acid-catalyzed.[1,2,3,4] For the materials of interest here, these polar groups are considered as favorable hydration sites that will promote the property of water vapor transport that is desired for CWA-protective clothing. Molecular gas transport, as opposed to viscous fluid flow through a labyrinth of pores, or even the more restrictive condition of Knudsen transport, wherein channel size is small compared to the mean free path of the gas,[5] is a general goal. In molecular transport, diffusants interact more intimately with the medium, which in this case is dynamic as the PIB phase is above T_g, and molecular hopping is encouraged by long range chain relaxations.

The research described in this report is a step toward realizing these goals.

II. ORGANIC SYNTHESIS COMPONENT

A. BLOCK COPOLYMER SYNTHESIS

1. Introduction

The focus of this part of the project continues to be the synthesis of polystyrene-polyisobutylene-polystyrene (PS-PIB-PS) block copolymers (BCP). Recent research concerns the synthesis of BCP's with the potential for dramatically increased hydration degrees, and thus higher moisture transport capabilities, after inorganic modification. Most of the triblocks synthesized thus far have fallen within the range of 15-26 vol% PS. After sulfonation of approximately 20% of the styrene repeat units, and neutralization with benzyltrimethylammonium hydroxide, this places the vol% PS roughly within the range 20-34 %. These compositions are expected to yield cylindrical morphologies, and indeed, most BCP ionomers and nanocomposites to date have displayed cylinders. We hypothesize that hydration degree can be increased by increasing the level of sulfonation and/or by increasing the relative hard segment length such that the composition of the final nanocomposite falls within the range of lamellar morphologies. It is hypothesized that lamellar morphologies will yield the highest moisture transport capabilities while still maintaining nanocomposites with elastomeric properties. These morphology targets can be met by creation of primary BCP's (prior to sulfonation) with PS contents within the range 30 – 45 vol%.

Compositional analysis of PS-PIB-PS block copolymers containing relatively low styrene contents, discussed in the reports for Years 1 and 2, showed that a small fraction of the copolymer chains undergo intermolecular chain coupling reactions during the styrene polymerization. These reactions cause the formation of higher molecular weight pentablock (and higher) species as shown in Figure 1-II. Coupling is an inherent feature of the cationic polymerization of styrene co-initiated with $TiCl_4$, and PS-PIB-PS triblock copolymers will inevitably contain more or less of these higher molecular weight species. There are certain advantages and disadvantages that might accrue from the presence of these higher molecular weight contaminants. From a synthetic point of view, their presence complicates the structural characterization of the materials. Each coupling reaction terminates a growing chain, so there is deterioration in the living nature of the polymerization. Coupled products also would obviously cause the melt viscosity of the BCP to increase and would thus present an impediment to melt processing. They would have little or no negative effect if solution processing were employed. With regard to mechanical and membrane performance properties, the presence of coupled material could very well be advantageous. Since coupling is within the glassy PS blocks, the resulting covalent bonds would increase the cohesiveness of the dispersed phase, adding strength, without affecting the continuous rubbery phase.

It was expected, and quickly confirmed (see Report for 1997 Activities), that this side reaction is more prevalent in the synthesis of BCP's of high styrene content owing to the longer styrene blocks. It was also established that coupling could be minimized through the use of the methylcyclohexane (MCHex)/methyl chloride (MeCl) 60/40 (v/v) cosolvent system. which had been reported by others for $TiCl_4$-coinitiated polymerization

of styrene.[6,7] Based on these findings the latter co-solvent system was chosen for further synthetic efforts toward high styrene content BCP's.

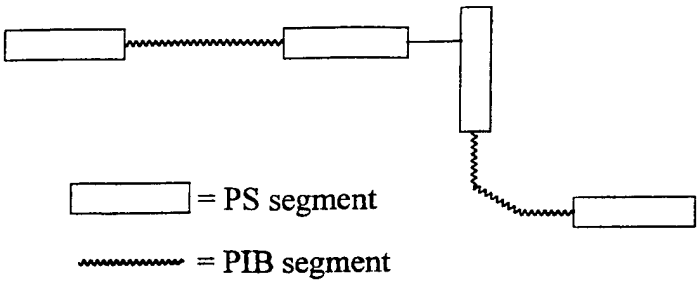

Figure 1-II. Typical product from intermolecular chain coupling reactions during styrene polymerization.

Our synthetic efforts on the polymerization of isobutylene and styrene have been greatly facilitated through our recent acquisition of a ReactIR™ 1000 reaction analysis system (real-time, remote, light conduit type ATR-FTIR spectrometer, ASI Applied Systems). This instrument was acquired through the DOD DURIP program and is equipped with a DiComp™ (diamond-composite) ATR (attenuated total reflectance) insertion probe, a general purpose PR-11 platinum resistance thermometer (RTD) and CN76000 series temperature controller (Omega Engineering). It is ideally suited for polymerization kinetics measurements by providing continuous monitoring of monomer concentration through collection of IR spectra of the polymerization components, and reactor temperature, in real time. We therefore have sought to integrate this powerful instrument into our program for synthesis of BCP's.

2. Experimental

a. Instrumentation

A ReactIR™ 1000 reaction analysis system (light conduit type) (ASI Applied Systems, Millersville, MD) equipped with a DiComp™ (diamond-composite) insertion probe, a general purpose type PR-11 platinum resistance thermometer (RTD) and CN76000 series temperature controller (Omega Engineering, Stamford, CT) was used to collect infrared spectra of the polymerization components, and monitor reactor temperature in real-time. (This instrument was obtained through the DURIP program of DOD.)

Polymerizations were carried out under dry nitrogen gas in a MBraun Labmaster 130 glove-box, equipped with an integral heptane bath cooled by both a FTS RC210 recirculating chiller (FTS Systems, Stone Ridge, NY) and liquid nitrogen, the latter regulated by a CN76000 series temperature controller (Omega Engineering, Stamford, CT).

a. Procedure

Cationic polymerization kinetics were determined as follows: Background spectra for use in ATR-FTIR analysis were obtained by fitting a stainless steel sleeve to the end of the DiComp™ probe of the ReactIR™ 1000 and immersing it in the heptane bath at -80 °C. After allowing sufficient time for thermal equilibration, a number of spectra were collected until a relatively constant peak profile was achieved. The sleeve was removed from the probe and replaced by a 250 mL four-neck round-bottom flask equipped with a mechanical stirrer and platinum resistance thermometer. The flask was then charged with 0.0676 g (1.17×10^{-3} mol) 1,3-di(2-chloro-2-propyl)-5-*tert*-butylbenzene (*t*-Bu-*m*-DCC) initiator, 110 mL MCHex, 73 mL MeCl, 9.2 x 10^{-2} mL (4×10^{-3} mol) 2,4-dimethyl-pyrindine, and 15.8 mL (0.2 mol) IB. The solution was stirred until thermal equilibration was reached as indicated by the thermometer (~10-15 min), and polymerization was initiated by the rapid addition of 1.4 mL (1.25×10^{-2} mol) of $TiCl_4$ (neat and at room temperature). Temperature and ATR-FTIR data were collected with the ReactIR™ 1000 system during reagent addition and subsequent polymerization. The ATR-FTIR data were comprised of spectra collected as the average of either 128 or 512 scans, over the spectral ranges of 4000-2200 and 1900-650 cm^{-1}, with 8 or 4 cm^{-1} resolution. The consumption of isobutylene over time was monitored with the ReactIR™ 1000 reaction analysis system until full conversion was attained. At this point, a sample of the PIB inner block was obtained for GPC analysis by withdrawing a 5-10 mL aliquot from the reaction vessel and adding it to a scintillation vial containing 10 mL anhydrous MeOH (–80 °C). To the remainder of the reaction volume was added 10.3 mL (0.09 mol) of styrene (STY) monomer as a 3.0 M solution in MCHex / MeCl (60/40 v/v). The consumption of the styrene was monitored with the ReactIR™ 1000 and aliquots of the BCP were taken over time.

The aliquots were analyzed by GPC to determine peak molecular weight (M_p) and molecular weight distribution. Subtraction of the PIB inner block M_p from the total M_p of each of the BCP aliquots yielded the molecular weight of the PS outer blocks.

3. Results and Discussion

The ReactIR 1000 reaction analysis system was used to obtain kinetic data for isobutylene and styrene polymerizations *via* real-time, *in-situ* ATR-FTIR spectroscopy. Monitoring the intensity of characteristic peaks in the IR spectrum allows the calculation of monomer concentration as a function of time. Figures 2-II and 3-II contain partial FTIR spectra illustrating the major absorbances of isobutylene and styrene monomer, respectively.

By monitoring specific peaks before and after polymerization is initiated (887 cm^{-1} for isobutylene and 910 cm^{-1} for styrene), a profile of the rate of monomer consumption over time can be constructed. Figure 4-II plots the relative intensity of the 887 cm^{-1} peak of isobutylene (measured as peak height; partial peak area yields essentially the same result)[8] versus time. The various events defining the course of the reaction are annotated in the figure, including the baseline absorbance prior to introduction of IB (solvent background signal), the absorbance at the initial isobutylene concentration [IB] = 1.0 M, and the initiation of the reaction upon addition of $TiCl_4$.

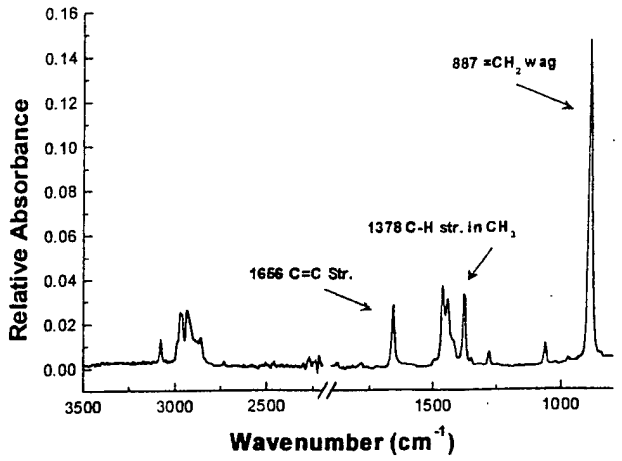

Figure 2-II. Partial FTIR spectrum of isobutylene illustrating major absorbances

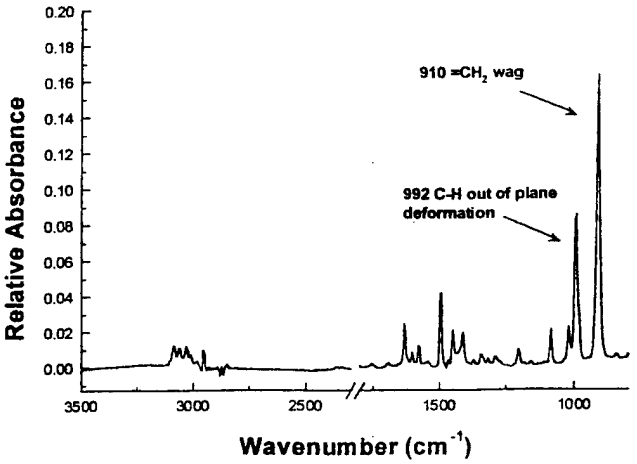

Figure 3-II. Partial FTIR spectrum of styrene illustrating major absorbances

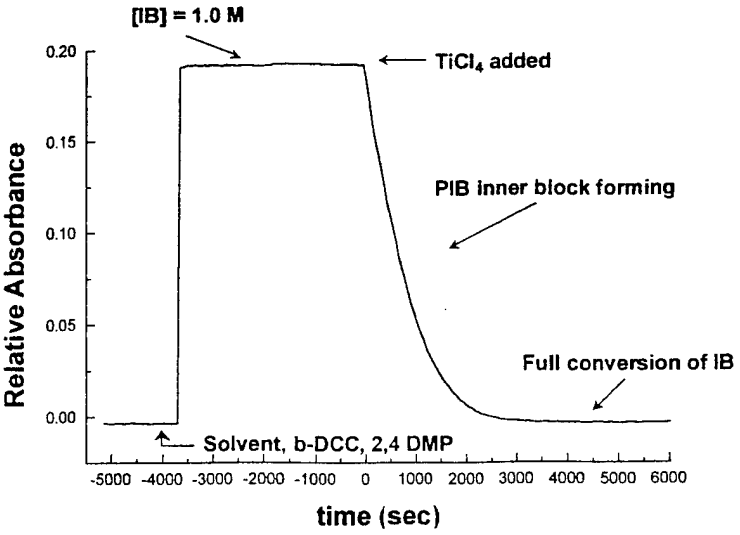

Figure 4-II. Profile of isobutylene monomer depletion over time, from analysis of absorbance at 887 cm^{-1}

The absorbance data were converted to concentration using $[M]_t = A_t - A_b$, where $[M]_t$ and A_t are the monomer concentration and relative absorbance, respectively, at time t and A_b is the background absorbance measured prior to introduction of IB to the reactor. (Alternatively, A_b may be taken as the absorbance at $t = \infty$, after complete reaction of the monomer.) The data were interpreted in terms of the kinetic rate law for a controlled/living polymerization with fast initiation:

$$r_p = -\frac{d[M]}{dt} = k_p[R^{\oplus}][M] = k_{app}[M] \qquad (1\text{-II})$$

where r_p is the rate of polymerization. k_p is the second-order rate constant for propagation. $[R^{\oplus}]$ is the concentration of instantaneously active growing chains (constant), k_{app} is the apparent rate constant for propagation, and [M] is the concentration of monomer. The concentration data obtained from Figures 4-II were then used to construct a first-order kinetic plot, shown in Figure 5-II, using the integrated form of Equation **(1)**, $\ln([M]_o/[M]_t)$ versus time. The slope of this line, the apparent rate constant for propagation, is denoted k_{app} and is equal to $k_p[R^{\oplus}]$. Although the data clearly show curvature, the origin of which is discussed below, they can be fitted reasonably to a straight line (depicted) whose slope is 1.7×10^{-3} s^{-1}.

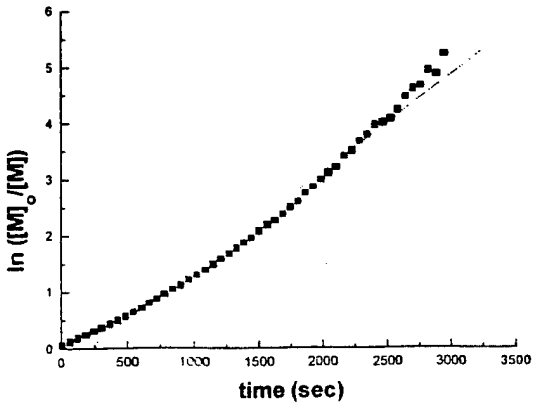

Figure 5-II. First-order kinetic plot of isobutylene polymerization.

The curvature in Figure 5-II is easily understood by consideration of the internal reactor temperature as a function of time, as shown in Figure 6-II. This data is also collected in real time and recorded by the ReactIR 1000. It was observed that the initial polymerization exotherm caused a rapid increase in the internal reactor temperature to about -77°C. Then, over a period of about 1,300 s the temperature gradually dropped as heat was transferred to the external cooling bath. At this point liquid N_2 was supplied to the external bath via thermostatic control, and the temperature returned to –80°C by about 2,000 s. The overall effect of this process is that the polymerization reaction was actually carried out in the range –78-(–77)°C during the first 1,500 s or so. The apparent activation energy for IB polymerization under these conditions has been measured to be –8.5 kcal/mole;[9] thus the apparent rate constant would be expected to be about 25% lower during this period than it would be had the

temperature remained constant at –80°C. Closer examination of Figure 6-II shows that indeed the slope of the curve is lower during the initial period up to about 1,500 s and then increases and remains approximately linear for the remainder of the reaction. Linear regression of the data from 0-1,500 s yielded a slope of 1.3×10^{-3}, which is about 38% lower than the slope of 2.1×10^{-3} for the data from 1,500 s on. This strongly suggests that the curvature is caused primarily by the temperature profile during polymerization.

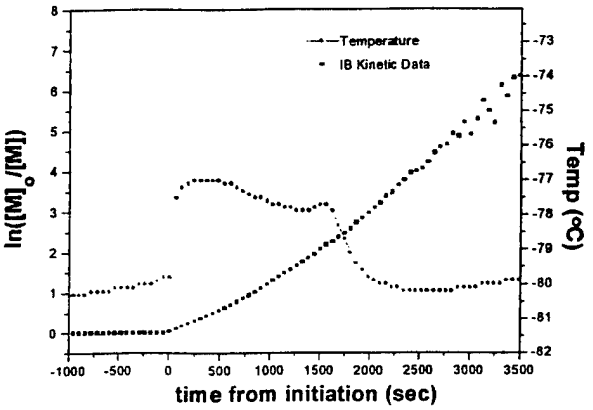

Figure 6-II. Internal reactor temperature as a function of reaction time during IB polymerization.

Monitoring of the styrene polymerization is rendered more difficult by the impossibility of obtaining a steady value for the initial styrene concentration. This results because the styrene necessarily must be added to a living solution for block copolymer synthesis, and thus the first data point is recorded after a finite amount of styrene has already reacted. Figure 7-II plots the relative intensity of the 910 cm^{-1} peak of styrene (measured as peak height) versus time elapsed after injection of styrene. The latter was carried out at a total reaction time of 118 min (17 half lives for the IB polymerization).

From Figure 7-II, concentraton data were calculated using the absorbance at $t = \infty$ as the value for A_b. The first-order kinetic plot for the polymerization of the styrene blocks is illustrated in Figure 8-II. The highest point recorded in Figure 7-II was taken as $[M]_o$ for styrene, and it should be noted that this is an underestimation. This error does not affect k_{app}, but it does cause an underestimation of the styrene conversion, which is important in the low-conversion regime. The k_{app} was measured to be 7.1×10^{-4} s^{-1}. The styrene polymerization was allowed to proceed for 158 min, during which aliquots of the BCP were taken at various times in order to evaluate the degree of coupling that had occurred as a function of styrene conversion. The reaction was terminated after a total reaction time of 276 min.

An advantage of using *in-situ* FTIR analysis to monitor BCP formation is that theoretically one can polymerize the monomer comprising the inner segment to a desired conversion, add the charge of a second monomer, and then continue the polymerization to yield a desired outer block length. Such synthetic flexibility obviates the need for a large body of kinetic data for a given system and greatly reduces the number of experiments necessary to obtain a BCP with the desired architecture. Table 1-II presents data on the peak molecular weights of the PIB inner block (PIB M_p) and the total BCP

(BCP M_p), and the calculated molecular weight of the PS outer blocks as determined by GPC analysis of aliquots taken during the polymerization. Listed in Table 2-II are the theoretical molecular weights of the PS segments based on conversion of styrene determined by *in-situ* FTIR analysis.

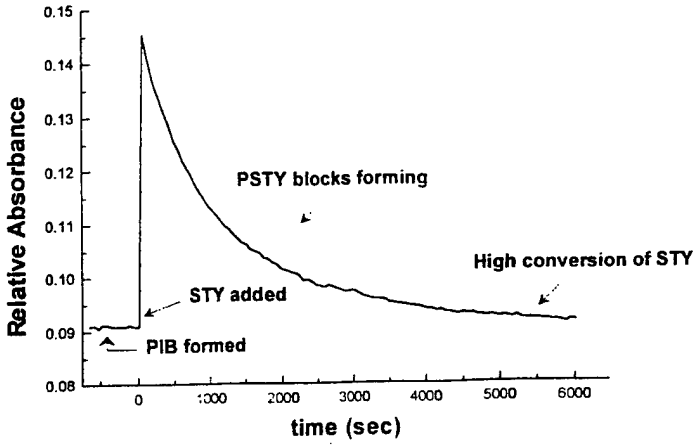

Figure 7-II. Profile of styrene monomer depletion over time from analysis of absorbance at 910 $cm.^{-1}$

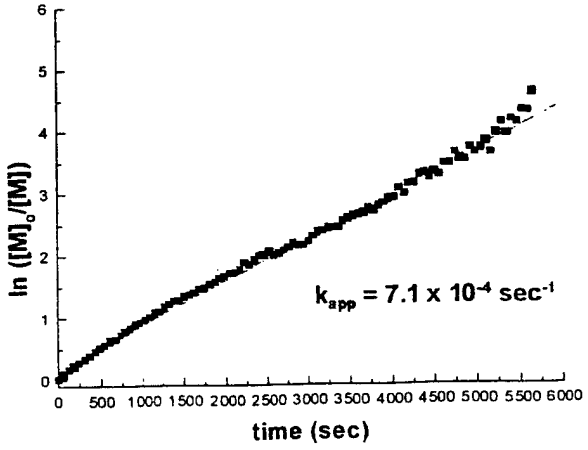

Figure 8-II. First-order kinetic plot for styrene polymerization.

Table1-II. Molecular weight data determined by GPC analysis of aliquots taken during BCP synthesis

Sample	Time (min) Styene Pzn.	PS wt% (from GPC)	PIB M_p (g/mol x 10^{-3})	BCP M_p (g/mol x 10^{-3})	PS M_p (g/mol x 10^{-3})
1	-	-		-	-
2	30	33		73.0	12.0
3	47	35	49.0	77.0	14.0
4	65	38		79.0	15.0
5	81	42		84.0	17.5
6	158	43		86.0	18.5

Table 2-II. Styrene conversion and PS block molecular weights calculated from ReactIR data of aliquots taken during BCP synthesis

Sample	% Conversion Styrene	PS M_n (g/mol x 10^{-3})
1	0	-
2	75	15.0
3	88	17.6
4	95	19.0
5	97	19.4
6	≈100	20.0

The BCP under discussion was designed to have an inner PIB segment of 48,000 g/mol, with PS outer segments of 16,000 g/mol. Such architecture would yield a BCP composed of 40 wt% styrene. In an attempt to minimize intermolecular coupling, excess styrene was added such that 80% conversion of the styrene charge would yield the desired PS blocks length. The PIB inner block was polymerized to complete conversion as indicated by *in-situ* FTIR analysis and was very close to its designed molecular weight of 48,000 g/mol. However, there is some discrepancy between the values of the molecular weight of the styrene segment determined by GPC and the values expected based on styrene consumption from *in-situ* FTIR analysis. This may be due to the inherent problems of determining molecular weights of BCPs by GPC, namely the determination of accurate dn/dc values for copolymers.

Molecular weights reported for GPC are determined from a Debye plot of data at the peak of the light scattering trace. The reason for this convention is evident upon viewing the GPC traces of the BCP aliquots presented in Figure 9-II. As anticipated, the longer styrene segments of the target BCP cause a rather high degree of intermolecular chain coupling. This makes it difficult to determine an average molecular weight that accurately reflects the target molecule: thus peak molecular weights, M_p, are reported. The GPC traces reveal that significant coupling had occurred after only 30 min of reaction of the styrene charge and that coupling increased with increasing reaction time. This reaction was purposefully carried to full conversion to observe the full extent of coupling. However, it is clear that the real-time FTIR monitor can be used to accurately time the termination of polymerization at any pre-determined conversion, and thus avoid the major amount of coupling that takes place at high conversion.

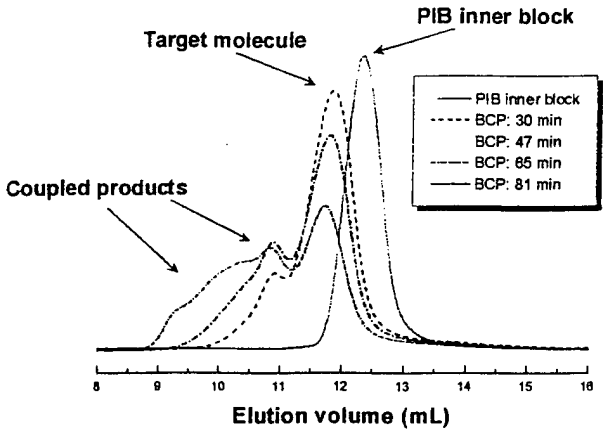

Figure 9-II. GPC traces (refractive index detector) of aliquots taken at various times during styrene polymerization.

B. SYNTHESIS OF TRIETHOXYSILYL-TELECHELIC PIB

1. Introduction

Initial efforts for the production of triethoxysilane-terminated PIB utilized exclusively hydrosilylation reactions between low molecular weight (2500 g/mol), allyl-terminal PIB and various silanes, namely trichlorosilane and triethoxysilane (see Report for1997 Activities). All of the attempted hydrosilylations employed a transition metal catalyst such as hexachloroplatinic acid (H_2PtCl_6). These reactions were performed in a number of polar and non-polar organic solvents, with many variations in reactant and catalyst concentrations. All reactions were performed either at room temperature or solvent reflux conditions.

The most successful reactions appeared to produce quantitative conversion of allyl-terminal PIB to alkoxysilyl-terminal PIB (as monitored by ^1H NMR) but were complicated by varying degrees of chain-chain coupling. The latter was attributed to condensation of ethoxysilyl groups catalyzed by combinations of trace amounts of water and acid that presumably were introduced with the solvent or hydrosilylation catalyst. Recent work has examined various combinations of solvents, e.g. toluene and 1,2-dichloroethane, and the different hydrosilylation catalysts listed in Table 3-II.

Table 3-II. Hydrosilylation Catalysts Investigated

H_2PtCl_6 (Control)
$Co(CO)_8$
Platinum divinyltetramethyldisiloxane complex (Karsted's Catalyst)
Chlorotris(triphenylphosphine)rhodium (I) (Wilkinson's Catalyst),
Platinum on activated carbon (Pt/C).

Hydrosilylation model studies using triethoxysilane, H_2PtCl_6, and 4,4,6,6-tetramethyl-1-heptene (TMP-allyl) to mimic the allyl-terminal PIB have been performed in order to better elucidate the hydrosilylation products obtained under more favorable reaction conditions. Alternate attempts have been made to obtain triethoxysilyl-telechelic

PIB by employing a urethane-forming reaction between γ–isocyanatopropyl triethoxysilane and alcohol-terminated PIB.

2. Experimental

All hydrosilylation reactions were conducted with either allyl-terminated difunctional PIB (Mn ≈ 2500 g/mol), initiated by *t*-Bu-*m*-DCC, or 4,4,6,6-tetramethyl-1-heptene (TMP-allyl), produced by the reaction of 2-chloro-2,4,4-trimethylpentane (TMPCl) and allyltrimethylsilane (Figure 10-II). The allyl-terminated PIB was dried by dissolution in hexanes, equilibration of the resulting solution over anhydrous $MgSO_4$, and final isolation of the polymer by vacuum stripping. The TMP-allyl was dried over CaH_2 and distilled under vacuum prior to use. All reactions were performed in 250 mL or 500 mL round-bottom flasks equipped with a mechanical stirrer and dry N_2 inlet port. For all reactions employing allyl-terminated PIB, a constant reaction stoichiometry was used with PIB:triethoxysilane:catalyst = 1:5:0.05; however, within the model hydrosilylations utilizing TMP-allyl, reaction stoichiometry TMP-allyl:triethoxysilane:catalyst varied from 1:1:0.05 to 1:5:0.05. All reaction solvents were dried by distillation from CaH_2. The PIB and TMP-allyl concentrations were constant at [PIB] = 0.024 mol/L and [TMP-allyl] = 0.048 mol/L. The percentage of allyl conversion was measured by integration of the allyl multiplets at 5.0 ppm and 5.8 ppm within the ^1H NMR, and normalizing them to the aromatic initiator peak at 7.15 ppm.

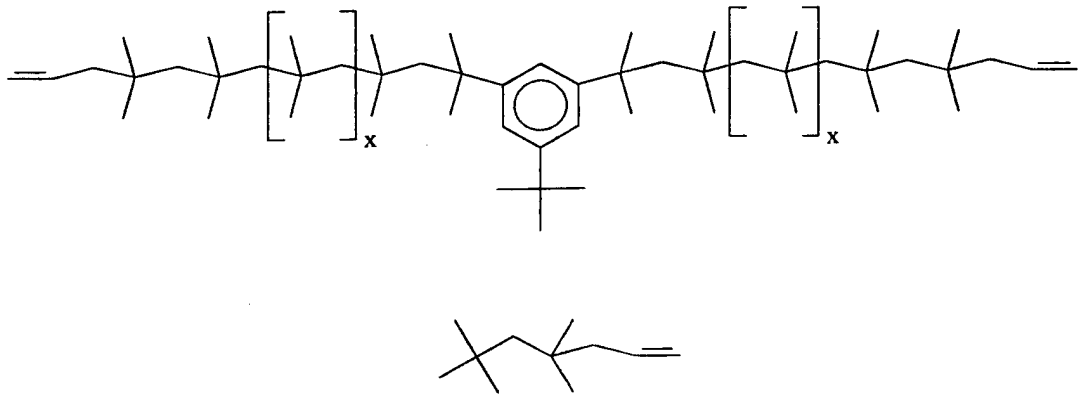

Figure 10-II. Difunctional allyl-terminated PIB (top) and TMP-Allyl (bottom).

Hydrosilylations catalyzed by platinum-divinyltetramethyldisiloxane complex (Karsted's Catalyst) were performed at room temperature, with all of the remaining reactions being carried out under reflux conditions. For hydrosilylations utilizing hexachloroplatinic acid, the catalyst was introduced into the reactor two separate ways: either solely by itself, or as a solution in 1,2-dimethoxyethane that was prepared with $H_2PtCl_6 \cdot 6H_2O$:ethanol:1,2-dimethoxyethane = 1:1:9. The ethanol and 1,2-dimethoxyethane were distilled from CaH_2 immediately prior to use. All other catalyst systems were utilized as received.

Urethane-forming reactions were attempted using difunctional hydroxy-terminal PIB, produced by the hydroboration/oxidation of allyl terminal PIB (2500 g/mol), and γ–

isocyanatopropyl triethoxysilane. which was vacuum distilled from $MgSO_4$ before use. Reaction stoichiometry was constant with [NCO]/[OH] = 2/1, and the PIB concentration was held at [PIB] = 0.048 mol/L. These reactions were performed under reflux conditions, using hexane as the solvent.

3. Results and Discussion

Previous reports discussed the intrinsic difficulty involved in the hydrosilylation reactions utilizing difunctional allyl-terminal PIB and triethoxysilane. The principal problem is chain-chain coupling that occurs within systems that exhibit high conversions of the PIB allyl-terminus. Chain coupling was attributed to condensation polymerization of the ethoxysilyl groups after attachment onto the PIB chains, and could be readily detected using GPC. It was hypothesized that trace amounts of water, along with a sufficient level of acidity from the hydrosilylation catalyst, were catalyzing the premature sol-gel condensation reactions. Since the PIB substrate and solvent were carefully dried prior to use, it was concluded that these impurities were introduced into the system via the catalyst. Further exhaustive measures were taken to eliminate possible acid and moisture sources by even more rigorous solvent purification and storage, along with changes to non-acidic hydrosilylation catalyst systems. Furthermore, two other solvent systems were used (i.e. toluene and 1,2-dichloroethane) in order to perhaps find a system that exhibited high degrees of hydrosilylation while simultaneously deterring sol-gel condensation. These two solvent systems showed marked differences in their hydrosilylation behavior with the 1,2-dichloroethane allowing only 5% allyl conversion after 48 h, and the toluene giving complete allyl conversion (> 98%) within 12 h. Although the toluene systems showed the highest hydrosilylation efficacy of any solvent thus far, no decrease in the levels of PIB chain-coupling was observed (Figure 11-II).

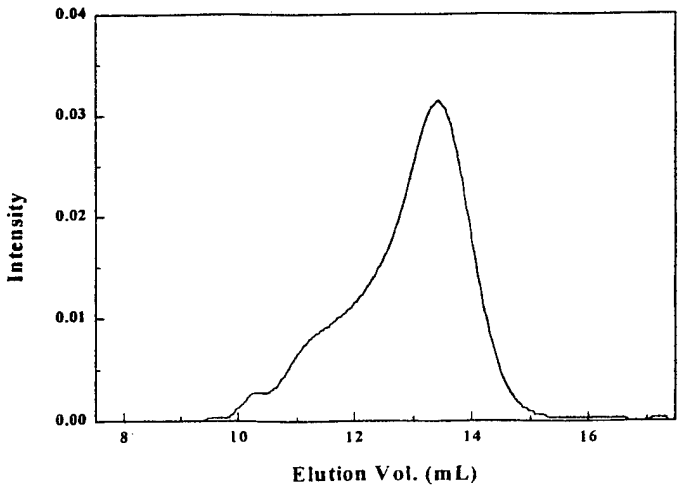

Figure 11-II. GPC chromatogram of toluene-solvated hydrosilylation

Literature research on the hydrosilylation of triethoxysilane and small molecule models that closely mimic the end group structure of allyl-terminal PIB (i.e., 1-alkenes) identified a few catalyst systems that might serve as possible non-acidic candidates.[10..12] After toluene was established as the most efficient solvent, each of the catalyst systems

list in Table 3-II was examined in terms of its hydrosilylation efficiency. Only two systems showed promise: hexachloroplatinic acid and platinum-divinyltetramethyldisiloxane complex (Karsted's Catalyst). Each of the other systems exhibited less than 5% allyl conversion within 48 h. Hydrosilylations using Karsted's catalyst reached >98% allyl conversion; however, it took nearly 72 h to attain this level. GPC evaluation of the resultant material revealed that there was no coupled product within the sample; however, there were two notable aspects of the ^{1}H NMR spectrum of the polymer product (Figure 12-II). Firstly, integration of the multiplet centered at 3.81 ppm, which has been attributed to the methylene units of the ethoxysilyl end groups, accounted for <10% of the PIB chain ends. Secondly, new olefinic resonances appeared at 5.25 ppm and 5.5 ppm. Evaluation of the ^{1}H NMR spectra of the H_2PtCl_6-catalyzed hydrosilylations reveals similar resonances that had been earlier attributed to the Si-H peak of unsatisfactorily cleaned samples.

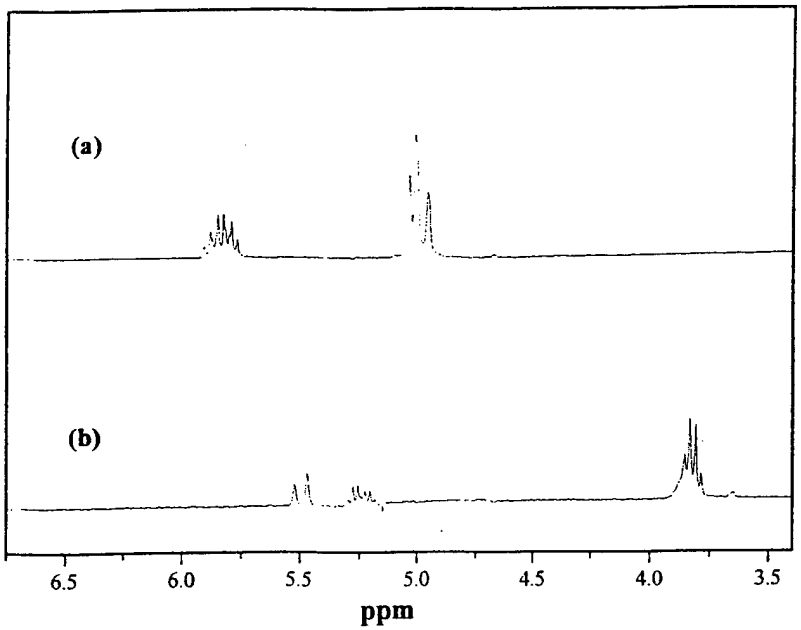

Figure 12-II. ^{1}H NMR spectrum of hydrosilylation catalyzed by Karsted's catalyst: (a) allyl-terminated PIB precursor, (b) crude product after 72 h reaction time.

Model hydrosilylation studies using TMP-allyl and triethoxysilane were performed to help elucidate the mechanistic features of these reactions. Three different catalysts systems were investigated: H_2PtCl_6 only, H_2PtCl_6/1,2-dimethoxyethane/ethanol, and Karsted's catalyst. After variations in stoichiometry and temperature were accounted for, all three of the catalyst systems displayed similar behavior to that illustrated in Figure 12-II. Further investigations also revealed that H_2PtCl_6-catalyzed reactions proceed with the fastest rate of allyl conversion; however, they also showed the highest amount of unidentified olefin resonances. Examination of the aliphatic region of the TMP-allyl model reactions further showed a larger extent of structural alterations for the H_2PtCl_6-catalyzed systems compared to the others.

Subsequent literature research revealed a plausible explanation for these results.[13] It is pertinent to note that side reactions that accompany metal complex-catalyzed

hydrosilylations involve compounds with one or more double bonds. Marciniec[13] explains that these reactions include isomerization, hydrogenation, and oligomerization via metathesis. Studies have shown that the presence of a particular type of silane markedly affects such reactions, which occur concurrently with hydrosilylation. Double-bond migration, shown in Figure 13-II, is a characteristic feature of most coordination catalytic reactions and can be viewed as a side-reaction occurring during hydrosilylation. It is further reported that the process of isomerization and hydrogenation is considerably faster than that of hydrosilylation, particularly when trichloro-substituted silanes are involved, and that during the addition of a trialkoxysilane to a 1-alkene an olefin-like isomerization is observed. It thus appears likely that isomerization to more hindered, and possibly less reactive, double bonds, and hydrogenation catalyzed by the platinum-based complexes, are both limiting the degree of hydrosilylation within these systems. Furthermore, uncontrollable metathesis reactions may be occurring simultaneously with hydrosilylation, which could explain the chain-chain coupling observed even with rigorously purified systems. With these findings in mind, it was deemed prudent to search for other synthetic schemes to produce the desired alkoxysilyl-telechelic PIB.

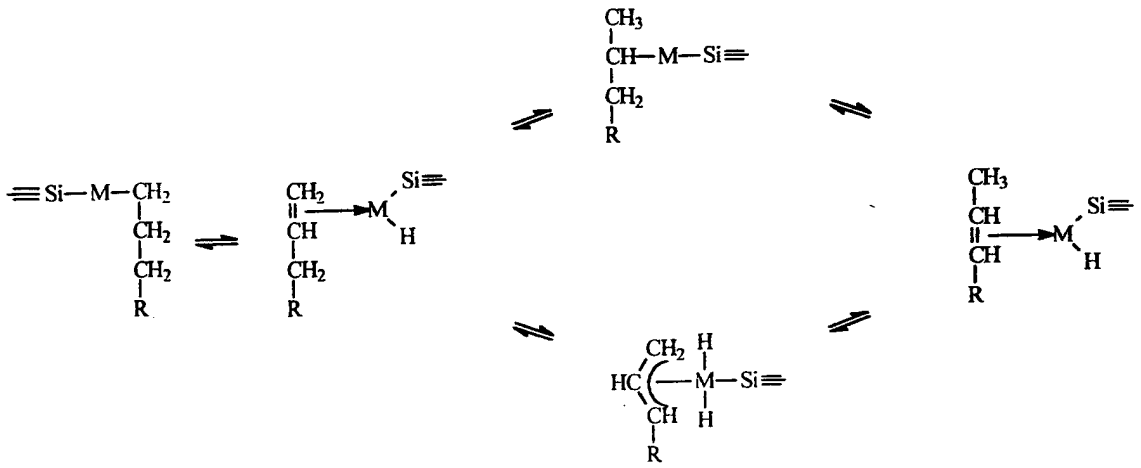

Figure 13-II. Double bond migration during hydrosilylation

Although hydrosilylation has thus far proven to be a disappointment in the synthesis of the desired materials, another promising possibility has been examined, which involves a urethane-forming reaction. In our previous report it was reported that Kaddami *et al.*[14] have synthesized triethoxysilyl-telechelic hydrogenated polybutadiene (H-PBD) through a reaction between γ–isocyanatopropyl triethoxysilane and alcohol-terminal H-PBD. Scouting experiments under similar conditions have yielded the desired triethoxysilyl-telechelic PIB. The synthetic scheme is shown in Figure 14-II.

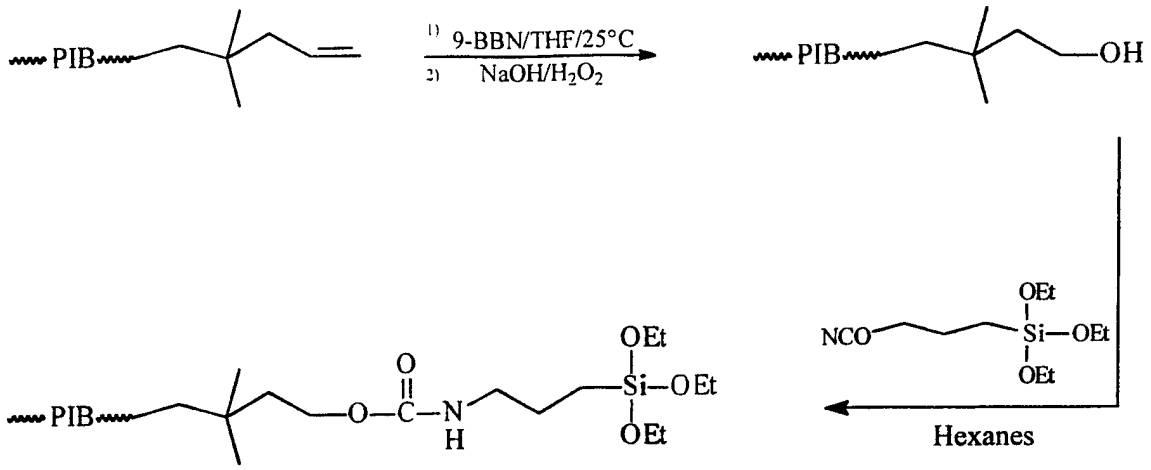

Figure 14-II. Synthesis of triethoxysilyl-telechelic PIB via urethane-forming reaction

Initial ^{1}H NMR investigations (Figure 15-II) of this urethane-forming reaction confirm the appearance of two multiplets centered at 3.2 ppm and 4.0 ppm corresponding to methylene units adjacent to –NH– and –COO– functionalities, respectively. Furthermore, the disappearance of the characteristic triplet of the methylene unit adjacent to the hydroxy-terminus of the alcohol-terminated PIB starting product (3.65 ppm) suggests complete conversion to the desired triethoxysilyl-terminated derivative. Product evaluation by GPC revealed that no chain-chain coupling occurred. Future experiments will be performed to identify the solvent condition, reaction temperature, and reaction stoichiometry needed to maximize yield and minimize subsequent cleanup procedures.

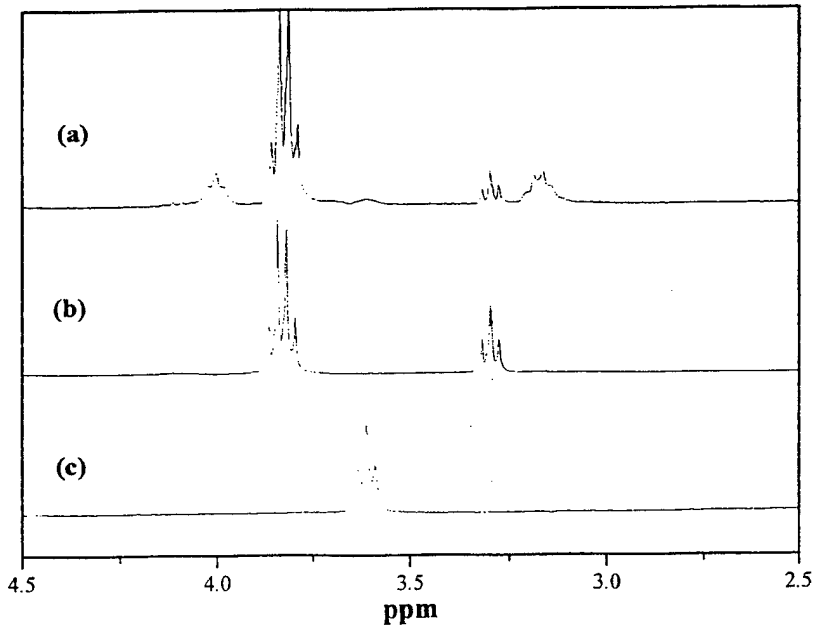

Figure 15-II. ^{1}H NMR of urethane-forming reaction: (a) crude product after 12 h reaction time (25 °C), (b) γ-isocyanatopropyl triethoxysilane, (c) alcohol-terminated PIB precusor.

III. INORGANIC MODIFICATION COMPONENT

A. EXPERIMENTAL (NANOCOMPOSITE FORMATION)

1. PS -PIB-PS Linear Triblock Copolymer Synthesis

The linear block copolymers (BCPs) used in these particular studies were constructed by living cationic polymerization using a method described elsewhere.[15] The molecular weight (M) and polydispersity index (PDI) of each polymer was determined via a GPC unit equipped with refractive index, laser light scattering, and UV detectors. ^{1}H NMR was used to determine the PS content. The results of this molecular weight characterization are summarized in Table 1-III below. It is anticipated that the styrene content is such that polystyrene cylinders or lamellae will exist in a PIB matrix.[16] This morphology is considered as necessary for the use of these materials as permselective, elastomeric materials.

Table 1-III. Composition and PDI of the BCPs used as TEOS sol-gel polymerization templates.

Block Copolymer	BCP M_n (kg/mol)	BCP M_w (kg/mol)	PDI	PS M_n (kg/mol)	% PS (Mol/ Vol/ Wt)
A	63.8	74.0	1.16	14.6	15.0/ 22.2/ 24.7
B	62.2	76.9	1.24	21.5	17.3/ 26.0/ 28.0
C	53.6	95.6	1.78	26.1	34.3/ 45.8/ 49.2

2. Procedure for Sulfonation of Poly(styrene-*b*-isobutylene-*b*-styrene)

Sulfonation of the BCPs was performed based on the method of Weiss *et al.*[17] A representative example of the procedure is as follows. Dichloroethane (110mL) and BCP B (10g) were added to a 250mL 3-neck flask equipped with a stirbar. The vessel was purged with nitrogen gas and placed in a 50°C oil bath. When the polymer was dissolved into solution, 1N acetyl sulfate (8mL) was added to the flask. The reaction was stopped after 2h by adding methanol to the flask (10mL). The sulfonated polymer was then isolated by steam stripping. The rubber crumb obtained from the stripping process was redissolved in dichloroethane (100mL) and steam stripped again. The polymer was then collected and stirred in hot water (1000mL) for 2h. The polymer was dried with desiccant under vacuum at ambient temperature and was protected from exposure to light.

3. Titration of Sulfonated BCP

The titration method used was based on a procedure devised by Storey and Baugh.[18] Mole percent sulfonation was determined by dissolving approximately 0.5g of BCP in toluene (100mL) and n-hexanol (1mL). The solution was heated to 80°C and titrated to a phenolphthalein endpoint using benzyltrimethyl-ammonium hydroxide (BTMA)

dissolved in methanol (approximately 0.02N). The BTMA solution was standardized against solutions of p-toluenesulfonic acid.

4. Formation and Film-Casting of BCP Ionomers (BCPI)

The film-casting method used was based on a procedure also devised by Storey and Baugh[4] and is described by the following example. BCP A (8.00g), tetrachloroethylene (250mL), and n-hexanol (8.0mL) were added to a 250mL 3-neck flask equipped with a mechanical stirrer. The polymer solution was titrated to a phenolphthalein endpoint using a tetrabutylammonium hydroxide (TBA) solution (0.5N). The TBA was standardized against samples of p-toluenesulfonic acid. Then, the BCPI solution was poured into 2 pans (5cm x 8.3cm x 3.4cm) which were then covered with aluminum foil having several holes in it. The pans were put in a drying oven at 60°C under an atmosphere of nitrogen for at least 10d after which the films were annealed for 2-3d at 60°C, 1d at 130°C, and 6-9h at 150°C, all annealing steps being done under vacuum. The films had a thickness of 0.5-0.8mm and were free of voids and were translucent. The BCPI films made for this study had benzyltrimethyl ammonium, tetrabutylammonium, or sodium cations.

5. BCPI-*in Situ* Sol-Gel Reactions

BCPI/silicate composites were formulated according to the following method. BCPI solvent-cast film strips were swollen in dimethylacetamide (DMAc) for less than 1d to affect a solvent uptake > 140%. The reason for this solvent swelling step is to facilitate the permeation of hydrolyzed tetraethylorthosilicate (TEOS) monomer and the preferential migration of these molecules to the hard block domains that is made possible by this particular solvent, as explained in our previous report. Solvent uptake was determined by gravimetric analysis and calculated using the following equation:

$$\%\ uptake = \frac{swollen\ wt - initial\ wt}{initial\ wt} * 100\% \qquad (1\text{-III})$$

A sol-gel-reactive solution was prepared by combining DMAc, TEOS, and deionized water (pH adjusted to 1.2 with HCl using a pH meter). The initially cloudy mixture became clear within several minutes of vigorous stirring. Once the solution cleared, the swollen film and DMAc in which it resided were added to the TEOS solution. All sol-gel reactions were performed at ambient temperature. The film was removed from the solution after a certain period of time and dipped in an n-propanol bath to wash excess TEOS from the film surfaces. The BCPI was then dried for 1d at 60°C, then for 1-2d at 120°C, and finally at 4-8h at 150°C, the entire heating cycle being performed under vacuum. In all of the sol-gel reactions, the H_2O:TEOS mole ratio was 4 and the HCl:TEOS mole ratio was 5×10^{-3}.

The BCPI composites were visually examined by ESEM/EDS (ESEM = environmental scanning electron microscopy, EDS = energy dispersive x-ray spectroscopy) analyses to ensure that no pure silicate precipitated on the BCPI film surfaces, as described previously.[19] Percent silica uptake was determined by two

methods: gravimetric (simple weighing) and thermogravimetric analysis (TGA). Equation 2-III was used to calculate silicate mass uptake for the gravimetric method and equation 3-III for the TGA method. The BCPI char (burnt carbonaceous matter) correction refers to the mass remaining in the TGA pan at 600°C when a pure BCPI sample is run instead of a composite.

$$\%\ uptake = \frac{BCPI\ composite\ \ wt - BCPI\ wt}{BCPI\ wt} * 100\% \qquad (2\text{-III})$$

$$\%\ uptake = \%\ mass\ remaining\ at\ 600°C - BCPI\ char\ correction \qquad (3\text{-III})$$

Table 2-III. BCPIs and BCPI/silicate composites

Material	Parent BCP	Mole Percent Sulfonation	Counterion Type	Wt % Silicate Uptake (gravimetric)	Wt % Silicate Uptake (TGA)
BCPI A	A	19	$BTMA^+$	-	-
BCPI B	A	19	Na^+	-	-
BCPI C	B	16	TBA	-	-
BCPI D	C	21	TBA	-	-
BCPI Composite A	B	16	$BTMA^+$	8.5	11
BCPI Composite B	A	19	$BTMA^+$	9.1	14
BCPI Composite C	B	16	TBA+	7.1	13

B. STRUCTURE-PROPERTIES CHARACTERIZATION

1. Methods, Instruments

a. Water-Swelling

Small circular pieces (~60mg) of BCP C and an ionomer of BCPI D were punched out of two films of comparable thickness. Pieces of each material were placed into four vessels of deionized water that were held at temperatures of 23°C, 50°C, 75°C, and 100°C. The materials were periodically removed from the vessels, blotted dry, and weighed to determine percent water uptake and equation 1 was used to calculate the degree of swelling.

b. Instrumentation

Solid state ^{29}Si NMR spectroscopy was used to gain a measure of molecular connectivity within the silicate phase of composite A. A Bruker MSL-400 spectrometer operating at a frequency of 79.5MHz with a relaxation delay of 200s was used to obtain quantitative information regarding the four characteristic Q peaks that are the fingerprints of degree of Si atom substitution about SiO_4 tetrahedra in the incorporated silicate quasi-networks. Smoothing of the spectra and integration of the area under the peaks was accomplished with Grams Software (Version 4).

The degradation profiles of the BCPs, their ionomeric forms, and composites were determined via thermogravimetric analysis (TGA) using a Mettler thermal analysis work station equipped with a TGA850 unit. Profiles for the composites were used to determine percent silicate resulting from the BCPI-*in situ* sol-gel reactions. TGA scans were obtained over the range 30°C–800°C at 10°C/min. Differential scanning calorimetry (DSC) profiles were obtained using a Mettler thermal analysis workstation where data were collected with a DSC 30 and TC 15 controller. 1st and 2nd heating scans were run from -150 to 200°C at 10°C/min.

Dynamic mechanical analyses of the BCPs, BCPIs, and BCPI/silicate materials were conducted with the use of a Seiko Instruments SDM5600 Viscoelasticity Analysis System with a DMS 210 Tension Module. Test specimens were approximately 9.8mm wide, 0.5–0.9mm thick, with a gage length of 10mm. Samples underwent cyclic tensile deformation at a constant frequency of 1Hz over the temperature range –120°C to above 100°C and the values of the loss tangent (tan δ) and storage modulus (E') were determined .

Dielectric relaxation analyses were conducted for the BCP C and BCPI D films. An electrical impedance analyzer (Hewlett-Packard 4192A LF) was connected to a parallel plate test cell having two gold electrodes and film samples were sandwiched between these electrodes. Complex admittance (Y^*) and complex impedance (Z^*) parameters were determined over the frequency range 5Hz - 13MHz for an applied low-amplitude sinusoidal signal. Data were collected using a 5 mV signal and the temperature of the experiment was 23°C. The real and imaginary components of the complex permittivity ($\varepsilon^* = \varepsilon' - i\varepsilon''$) were derived from the impedance data using a previously reported equation.[20] The BCP film was evaluated in this way in the dry state and the BCPI film evaluated in both the dry and water-swollen states. The water-swollen film was blotted dry to ensure that good contact was established between the electrodes and the actual polymer rather than a water-adhered layer.

2. Results and Discussion

a. ^{29}Si Solid State NMR Spectroscopic Analysis of Silicate Phase Microstructure

Figure 1-III shows a ^{29}Si NMR spectrum of BCPI composite A. The four peaks are characteristic of $Q = Si(O_{1/2})$ groups that are incorporated into a silicate network by polycondensation reactions. These peaks, conventionally labeled as Q_1, Q_2, Q_3, and Q_4, refer to mono-, di-, tri-, and tetra-substitution of Si atoms about SiO_4 tetrahedra. For example, a large population of Q_4 species, quantified by a large relative area under this peak would indicate a rather highly connected network. On the other hand, an overwhelming area under the Q_2 peak would reflect long linear runs of molecular substructures. It should be kept in mind that these are necessary, but not sufficient conditions for these sort of network configurations.

In addition to elucidating the molecular structures of incorporated silicate nanophases, these spectra can give useful information related to this DOD application that requires the transport of water, arising from perspiration, across CWA-resistant materials. SiOH groups residing on the "surfaces" of silicate structures (see Figure 2-III) are envisioned as sites that attract water molecules, mainly through hydrogen bonding,

and such groups inserted along sulfonated PS domains will render the membrane very hydrophilic. If these polar domains are contiguous there will be continuous hydration pathways along which H_2O molecules can migrate. It might also be imagined that high chain segmental mobility within the PIB phase will facilitate water transport by influencing the molecular dynamics of contacting hydrate structures.

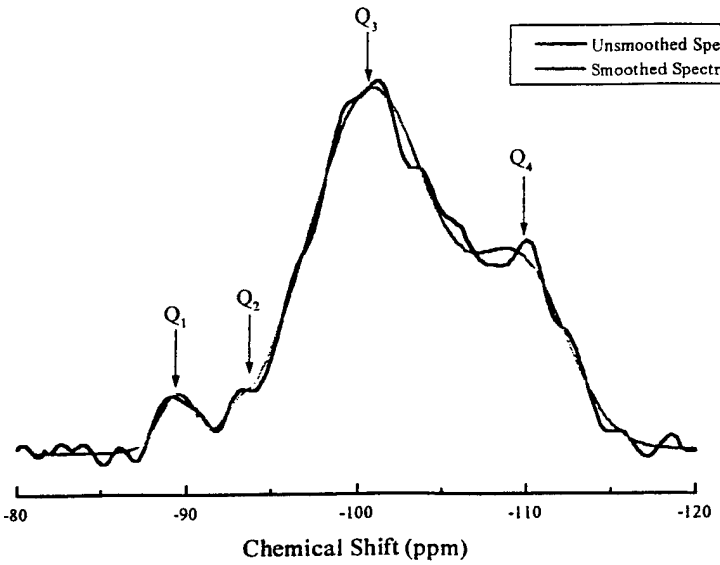

Peak	% Area
Q_1	13.0
Q_2	0.37
Q_3	65.4
Q_4	21.1

Figure 1-III. Solid state ^{29}Si NMR spectra of BCPI($BTMA^+$) composite A.

The normalized area analysis of the spectra, shown in Figure 1-III, shows that there is indeed a significant amount of Q_1-through-Q_3 species present in the inorganic phase so that a significant number of SiOH groups are indeed present.

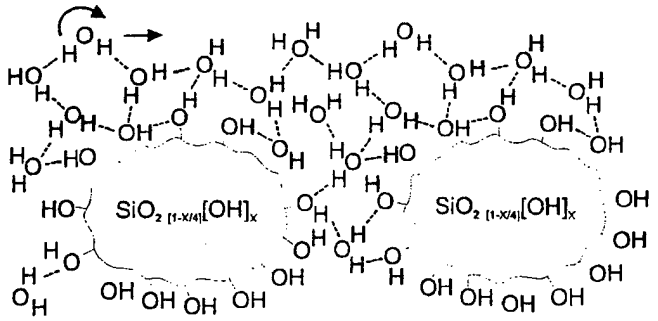

Figure 2-III. Crude depiction of the hydration of silicate nanostructures. H_2O molecules in the outer hydration shells are expected to be more mobile.

b. Thermogravimetric Analysis (Series I)

Table 2-III lists the compositions of the BCPIs and BCPI composites used in these studies. It is seen that the silicate uptake numbers measured by the gravimetric and TGA

methods do not agree. The TGA method always gives a number at least 2% higher than that for the gravimetric method. Perhaps low molecular weight polymer chains, which are sparingly present in the BCPs, were leached out of the material by the swelling solvent DMAc. The leaching would explain the discrepancy because it would affect the gravimetric but not the TGA method. Simple gravimetric analysis relies on the difference in mass before and after the sol-gel reaction, while the TGA method simply relies on the amount of material left after the BCPI matrix has been degraded. Studies are currently in progress to verify this idea by attempting to exact the low molecular weight material from the BCP before the *in situ* sol-gel reaction.

Figure 3-III consists of TGA profiles of ionomers and a composite derived from BCP A, including BCPI A, BCPI B, and BCPI composite B. With reference to the plot on the right, it is seen that the Na^+ form ionomer and the BCP have very similar degradation profiles indicating that Na^+ ions do not strongly influence degradation. However, the $BTMA^+$ ionomer does degrades faster than the BCP up to approximately 400°C where the profiles of the BCP and both ionic forms then largely coincide. At 400°C, the $BTMA^+$ BCPI lost ~12% mass, which is perhaps due to $BTMA^+$ ion decomposition. The scans on the left are for a BCP, BCPI, and BCPI composite having 14% silicate uptakes, where the ionomer and composite are in the $BTMA^+$ form. Incorporation of the silicate phase considerably hindered the degradation relative to the ionomer precursor between ~200°C and 400°C. It is suggested that the silicate phase inhibits decomposition of the $BTMA^+$ cations, perhaps by forming structures that surround $-SO_3^-$-$BTMA^+$ ion pairs. If so, the silicate phase would have to reside in/around PS domains near and not in the PIB phase, which, in fact, was a conclusion based on our earlier work.

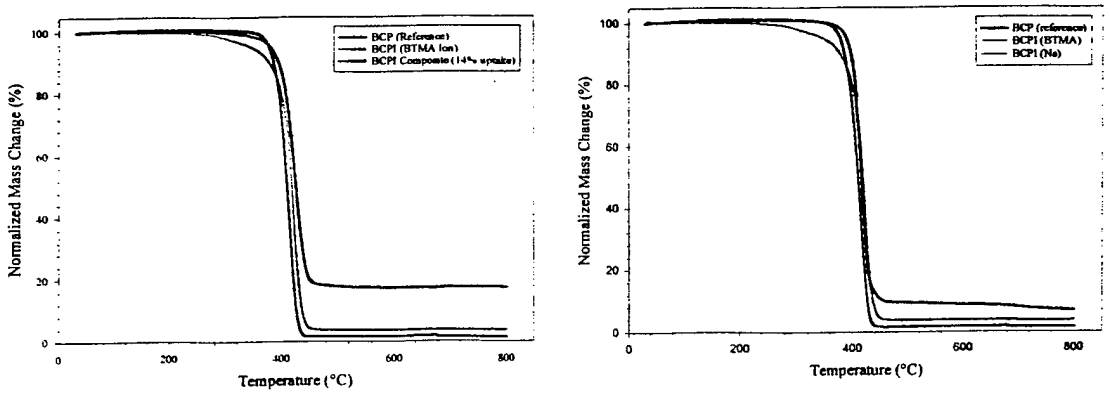

Figure 3-III. Left: TGA profiles of a 25% styrene BCP series consisting of BCP A, BCPI A, and BCPI composite B. Right: TGA profiles of a BCP and two ionomers (BCPI A and B) originating from the BCP A.

c. Differential Scanning Calorimetry

Figure 4-III shows 1st and 2nd DSC scans of BCPs having varying PS weight percents (BCPs A,B, and C). T_g for the PIB block is invariant vs. %PS, in agreement with our previous results for similar BCPs.[21] While it is not discernable for the 25 and 28% PS

compositions, the 49% PS sample exhibits a T_g for the styrene blocks, although it is still weak. The endotherm in the region 50-75°C of the first scan is interesting because it was not previously observed when the materials were melt pressed or solvent precipitated, instead of solvent-cast.

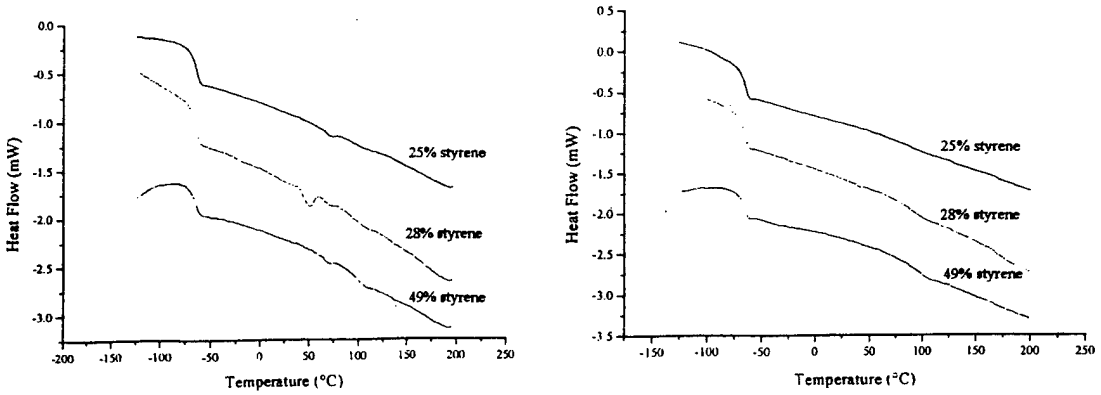

Figure 4-III. DSC scans of a BCP series of styrene weight percent. Left: first scans. Right: second scans. Curves are vertically displaced to allow for better comparison.

d. Dynamic Mechanical Analysis

Figure 5-III shows tan δ (top) and E' (bottom) vs. temperature curves for BCP B, BCPI C, and BCPI/silicate composite C. The tan δ curve for the unmodified BCP shows two distinct relaxations, one centered at approximately –50°C and the other at 100°C, which are assigned to the glass transitions of the PIB and PS domains, respectively.

The peak at –50°C is quite broad, for which we offer the following explanation. Plazek *et al.*[22], who performed viscoelastic studies of pure PIB, hold that this glass transition region is actually composed of two transitions, one corresponding to Rouse and the other to sub-Rouse chain motions. These segmental motions, especially the first, must be the primary mechanisms accounting for the peak region and low temperature tail in Figure 5-III. The studies of Baugh and Storey, of the more complicated PS-PIB-PS ionomers,[23] suggest that there is a higher temperature component attributed to the onset of segmental motions of more constrained PIB chains at the *interface* of the phase-separated domains. Compared to the unmodified BCP, there is considerably less area under the PIB glass transition peak for the ionomer and even less so for the corresponding silicate-incorporated ionomer. Obviously, for the ionomer, electrostatic interactions must be implicated in restriction of chain segmental mobility, although it is unclear as to how this occurs exactly. For the composite, embedded silicate structures might pose motional restrictions on PIB chain sections near the interfacial regions. Arguments of this sort might be based on the fact that the curve sections are depressed along the high temperature wings of the peak for the ionomer and composite. Moreover, the PIB phase T_g for the composite is slightly lowered relative to that of the ionomer, which might implicate the complete immobilization of PIB segments at the interface. However, the temperatures of the peak maxima, *i.e.*, the main T_g–related motions, are not

significantly affected by the incorporation of these ionic groups or by inclusion of the silicate phase. The latter fact provides additional evidence that the silicate phase is preferentially incorporated around the PS domains and not in the PIB phase. While the onset of the glass transition in each of the three cases occurs at essentially the same temperature, the concept of the progressive immobilization of chain segments in proceeding from the BCP to the BCPI to the composite is supported by the progressively smaller drop in E' at T_g in this order.

The PS glass transition is seen more distinctly for the ionomer than the BCP on the tan δ and E' curves and the ionomer exhibits another peak centered at ~175°C. We offer the speculation that this additional peak is due a division within PS domains between predominantly sulfonated and unsulfonated regions where there are motionally-restrictive electrostatic crosslinks within the former that produce a higher T_g as in simpler styrene ionomers.[24]

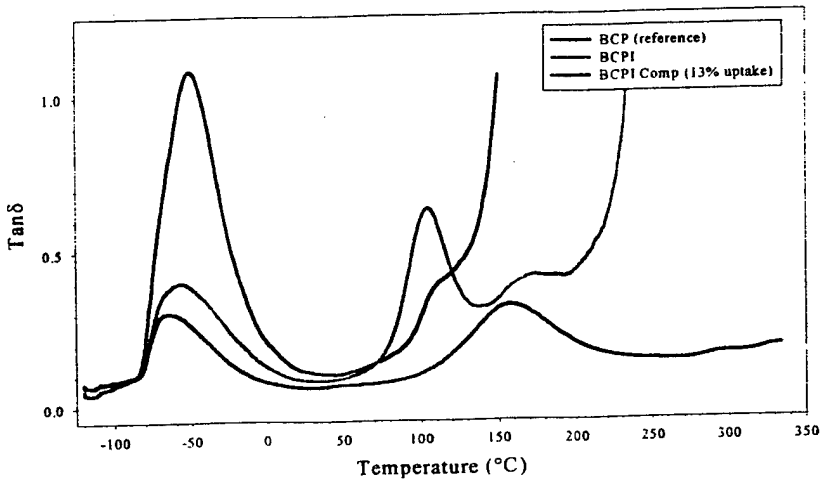

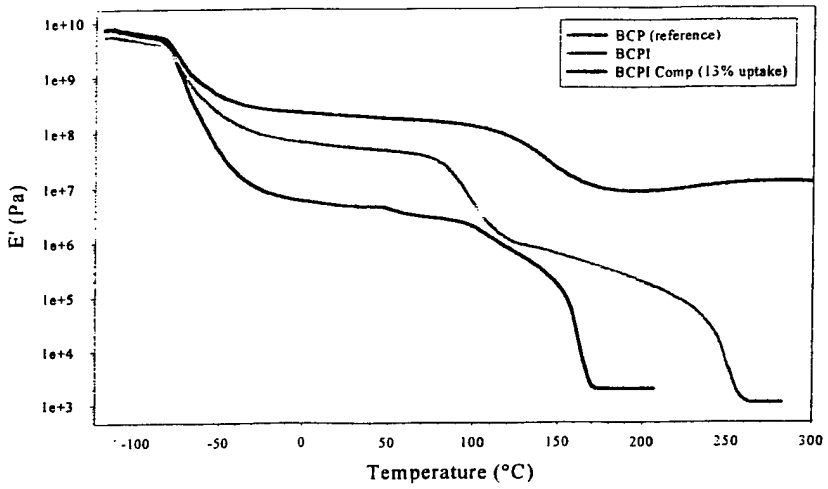

Figure 5-III. Dynamic mechanical loss tangent (top) and storage modulus (bottom) for BCP B, BCPI C, and BCPI composite C.

The curve for the composite indicates the absence of the PS T_g at 100°C but there is a broad transition over a temperature range 100-240°C that is also manifest by a drop in E'. We interpret this in terms of silicate particles have been preferentially incorporated around and perhaps into the PS domains so as to restrict chain segmental mobility therein.

On examining the rubbery plateau regions for the E' plots, it is seen that the BCP material can be made significantly stiffer by incorporating ions and then the silicate nanostructures.

e. Water Capacity

Figure 6-III consists of water uptake vs. immersion time curves for BCP C and BCPI D. Effectively, no uptake occurred at any temperature for the unmodified BCP, even after 50h exposure. The BCPI did absorb water, although the 50°C data is inconsistent with the rest. The data for 23°C and 75°C show that the ionomer absorbed at least 20% of its own weight. The rather high uptake at 100°C is rationalized in terms of the fact that this temperature is in the vicinity of the PS phase T_g and the greatly increased mobility of the PS chains are expected to enhance water permeation.

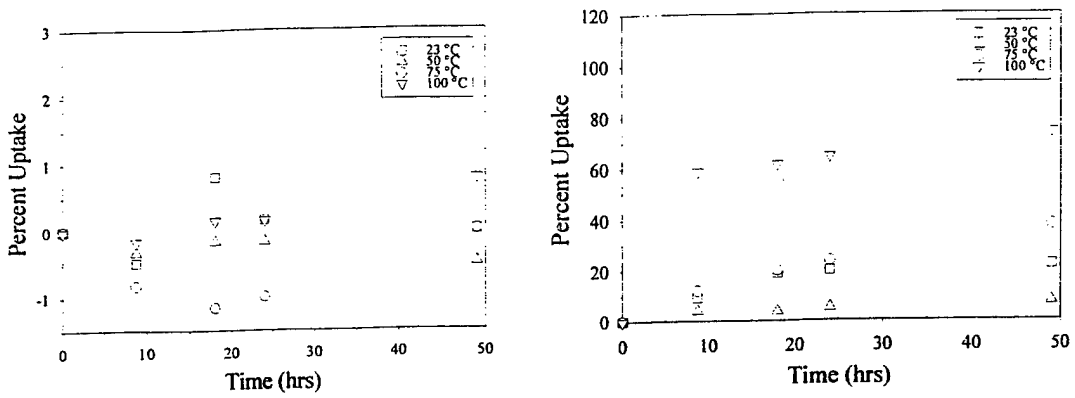

Figure 6-III. Water-swelling studies of a BCP C (left) and a BCPI D (right).

f. Dielectric Relaxation Spectroscopy

The technique of *dielectric relaxation* can probe long and short ranged molecular motions within polymer structures. However, when the polymer is imbibed with a large amount of water, the spectral manifestations of these relaxations can be overwhelmed by features that reflect the clustering and/or long range migration of water as well as the motions of free ions. The Cole-Cole plot for a BCPI film having 47% water uptake is shown in Figure 7-III. The data point progression from right to left corresponds to an increase in signal frequency f. There are two features to note on this curve. In the low frequency regime, a relaxation semicircle can be well-fitted to the curve. The relaxation time for this high frequency process, τ, is equal to $(2\pi f_{max})^{-1}$ where f_{max} is the frequency for which ε" is maximum. The time scale on which these molecular rearrangements occur is equal to $\tau = 2.12$ milliseconds. The fact that the center of this circle lies rather directly on the ε' axis means that there is no distribution of relaxation times about the value of τ for this process. Given this high water uptake. we offer the tentative suggestion that clusters of water must necessarily form around the ionic hard blocks. As the dielectric constant of these water clusters is considerably greater than that of the surrounding organic PIB phase it is not unreasonable to think that there is a relaxation of interfacial polarization that occurs within the time frame τ. This phenomenon for heterogeneous materials is referred to as the Maxwell-Wagner-Sillars effect and essentially involves the alternate accumulation and dissipation of electric charge (either mobile charges or unbalanced partial charges) at the phase boundaries which can lead to rather high dielectric constants.[25] The high permittivity values seen on the Cole–Cole plot certainly lend support to this idea. The fact that this relaxation time is rather long can be accounted for by considering that this process involves the cooperative motions of large aggregates of hydrogen bonded water molecules.

The upswing in the curve as it deviates from the semicircle region for monotonically decreasing frequencies might be attributed, in the usual way, to diffusion. In this case, it is visualized that the water clusters are contiguous and that H_2O molecules percolate along these hydration pathways. Given the validity of this concept, the technique of dielectric relaxation could be rather useful in probing water incorporation

and water transport, which is an important consideration within the context of the use of these materials as CWA barriers while allowing for the outward transport of water associated with perspiration.

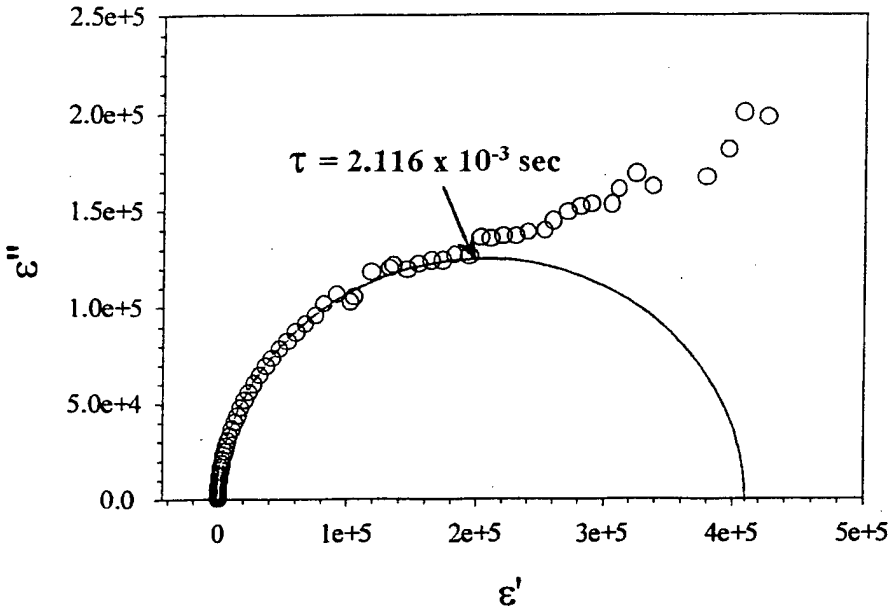

Figure 7-III. Cole-Cole plot for a water-swollen BCPI D film where the water uptake is 47%.

g. Thermogravimetric Analysis (Series II)

TGA experiments were conducted on BCPs, BCPIs and BCPI/silicate composites for materials that were of different composition than those reported in the above-described similar experiments (Series I). The results are reported here because they refer to the particular materials discussed in this section. Temperature was increased (one scan) from room temperature (25°C) to 800°C at 20°C/min. Sample sizes were between 10 and 20mg. Nonoxidative thermal degradation vs. temperature was affected and monitored in a N_2 atmosphere. Degradation temperatures, T_d, are reported as the onset of degradation as calculated from the intersection of the baseline defined by the straight curve near 100% sample mass and the line tangent to the inflection point in the region of catastrophic loss. In some cases, the inflection point was used as a measure of T_d when the baseline prior to catastrophic mass loss was not flat. We describe, below, a TGA analysis of a Na^+ form BCPI. The M_w for the parent BCP is 78,400 g/mol and the PS composition is 18 mole % of which 12.8 mole % has been sulfonated. The Na^+ form BCPI was prepared in the same manner as the $BTMA^+$ form BCPI that is mentioned elsewhere in this report. The base used to neutralize the sulfonic acid form BCP was

NaOH/methanol. Conditions for film casting and inorganic alkoxide (TEOS) incorporation were similar to those reported before.[26]

Table 3-III lists T_d for several parent BCPs of indicated overall molecular weights, polydispersities and mole percent PS. It is seen that T_d practically independent of molecular weight and copolymer composition over the respective, small ranges of these properties.

Table 3-III. T_d and inflection point values for the thermal degradation of the parent BCPs

M_n / M_w (x 10^{-3})	Mole % PS	T_d, °C	Inflection Point, °C
47.2 / 55.4	3.2	391.3	418.7
47.0 / 57.5	9.4	389.6	420.5
66.3 / 72.3	10.8	391.3	420.4
56.2 / 59.9	12.8	389.6	418.4
65.3 / 75.1	13.1	389.6	422.5
62.2 / 76.9	17.3	391.3	420.5
62.8 / 78.4	18	388.2	417.2

Figure 8-III consists of TGA scans for an unmodified BCP, the Na^+ BCPI, and two BCPI/silicate composites. In all cases the degradation, at least from a superficial gravimetric (rather than spectroscopic-molecular) perspective, occurs as a single catastrophic event rather than in multistep fashion notwithstanding the fact that this is a block copolymer, as well as to the fact that one of the blocks has been further differentiated by chemical modification.

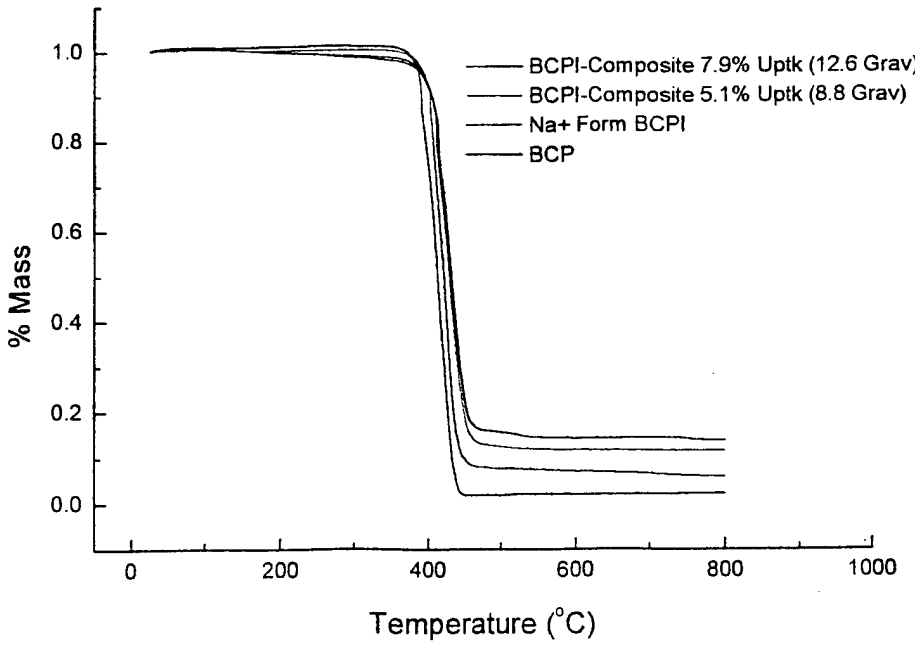

Figure 8-III. Degradation profiles for a series of BCP, Na^+ BCPI, and composites. As loading increases, degradation temperature increases with respect to both onset and inflection point.

Table 4-III lists T_d and the inflection point values for degradation profiles for a BCP, Na^+ BCPI and BCPI/silicate composites of various inorganic contents. It is seen that the

Table 4-III. Degradation parameters for BCP, Na^+ BCPI and composites

Sample Type	% Uptake TGA/Gravimetric	T_d, °C	Inflection Point, °C
BCP	0	388.2	417.2
Na^+ BCPI	0	398.9	423.5
Composite	1.5 / 2.6	397.2	425.4
Composite	2.2 / 3.5	398.9	425.2
Composite	5.2 / 5.3	406.5	429.1
Composite	5.1 / 8.8	403.4	428.6
Composite	6.1 / 5.19	403.4	429.2
Composite	6.6 / 7.8	401.7	430.5
Composite	7.2 / 10.8	404.8	431
Composite	7.3 / 11.9	406.5	433
Composite	7.9 / 12.6	404.8	431

ionomer T_d as well as inflection point is significantly elevated with respect to the pure BCP. This might be reasonably attributed to the influence of strong electrostatic interactions posed by the fixed ions. While there is some fluctuation in the data, T_d is increased further with incorporation of a silicate phase, although degradation products seem to evolve earlier in the temperature program. The slow mass loss prior to the catastrophic drop in mass can be attributed to both volatiles in the form of residual solvents (hexanol and DMAc from film casting) as well as water and ethanol that issue from temperature-driven condensation reactions between silicate-affixed Si-OH and Si-OEt groups. In general, the inflection point is shifted to higher temperatures. On the other hand, the shift in these temperatures is not so severe as to be due to a significant invasion of the PIB phase by silicate structures, as discussed elsewhere in this report.

As mentioned, % silicate uptake was determined gravimetrically (simple weighing) and by TGA. In the gravimetric case, the mass of the film is determined before and after the *in situ* sol-gel reaction for TEOS and subsequent drying and the measured mass increase is divided by the original mass (x 100%) to yield percent uptake. The TGA method compares the percent mass of the totally degraded BCPI film to that of the BCPI-composite after it. as well , is heated to the char state. The difference between these two masses is attributed to the silicate phase. It was noticed that the values by the two methods do not agree, the TGA uptake being *ca.* 2% smaller than that for the gravimetric value. Up to 2% of the mass of the BCP can be homo-PS or PIB-PS *diblock* material, and these fractions can be solubilized by DMAc solvent and leached out of the BCPI film during the *in situ* sol-gel process for TEOS. However, experiments performed in our labs show only minimal mass loss (< 1%) due to swelling a Na^+ form BCPI in DMAc with subsequent drying of the BCPI in a vacuum oven. Another contribution to the lower TGA value comes from the fact that the ultimate, high temperature-derived silicate residue is highly condensed so that a considerable number of reactive SiOH

groups have generated water. On the other hand, the gravimetric method measures the uptake of an internal silicate structure having only *ca.* 70 % conversion of reactive functional groups as seen in the section in this report dealing with Si^{29} NMR spectroscopy.

Table 5-III and Figure 9-III refer to the thermal degradation of PS and PIB homopolymers. T_d and inflection point values for PIB are in fact very close to those for the unmodified, more complex BCPs. While T_d for homopolystyrene is greater that of homopoly isobutylene, the presence the PS blocks in the BCP does not seem to raise the degradative stability of the BCP above that of pure PIB block. Also, the fact that the two curves in Figure 9-III are rather close to each other shows why the BCP curve does not *appear* as a two step process although the unzipping of the two distinct blocks occur somewhat simultaneously. On the other hand, modification of the PS block by affixing $SO_3^- Na^+$ ions as well as incorporating a silicate component, does in fact increase T_d.

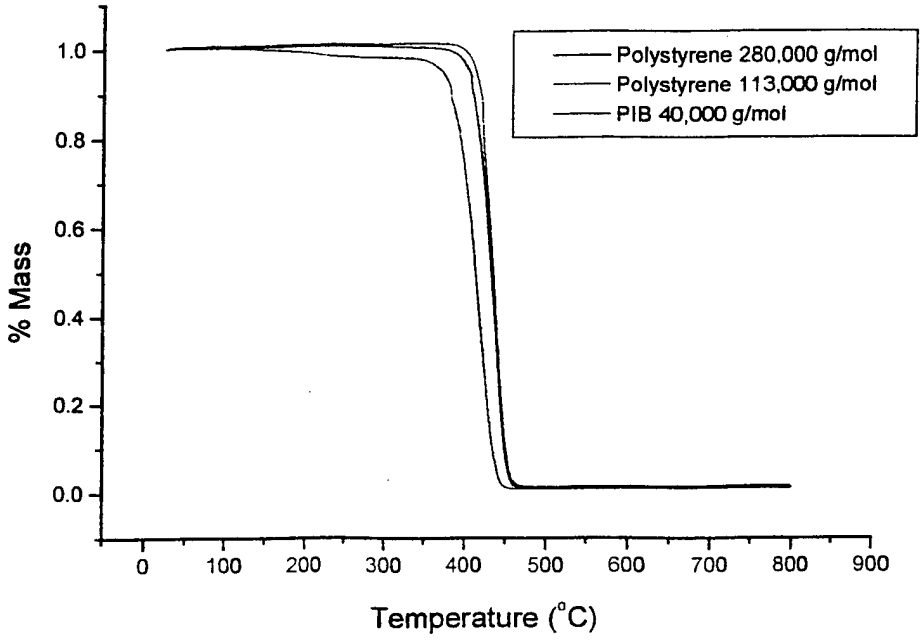

Figure 9-III. TGA curves for PS and PIB homopolymers.

Table 5-III. T_d for PS and PIB homopolymers

Sample	M_n (x 10^{-3})	T_d Onset, °C	Inflection Point, °C
PS	280	412	438.2
PS	113	416.3	438.9
PIB	40	388.8	420.3

h. TEM-AFM Studies of Morphology

Materials and Experimental. Microscopic analyses of a silicate-modified $BTMA^+$ form BCPI were performed. M_w for the parent BCP is 76,900 g/mol with 18 mole % PS repeat

units in blocks. The PS blocks were then sulfonated to the extent of 16 mole % PS. Transmission electron microscopy (TEM) and atomic force microscopy (AFM) were used to probe fine-scale morphology. The parent BCP is roughly 29% PS *by volume*. PS cylinders in a continuous PIB phase are theoretically expected for this composition. For the BCPI-composite, the PS phase volume fraction is further increased by sulfonation, and more so by subsequent silicate incorporation. Nonetheless, it will be demonstrated that cylindrical morphology is preserved after this chemical modification of the BCP.

Figure 10-III illustrates the preparation of samples that allows for meaningful comparison of AFM with TEM images in that two samples, not only from the same block, but immediately across from a cut through the solid state material. A BCPI sample was sectioned with a Richert Jung UltraCut E at -120°C using a diamond knife. Sections (RuO_4–stained and unstained), on the order of 100 nm thick, were collected on copper grids and then inspected with a Ziess10C TEM at a voltage of 60keV. The block face was analyzed by tapping mode AFM using a Digital Instruments D3000 with a silicon probe tip. All images presented here are 4μm full scale.

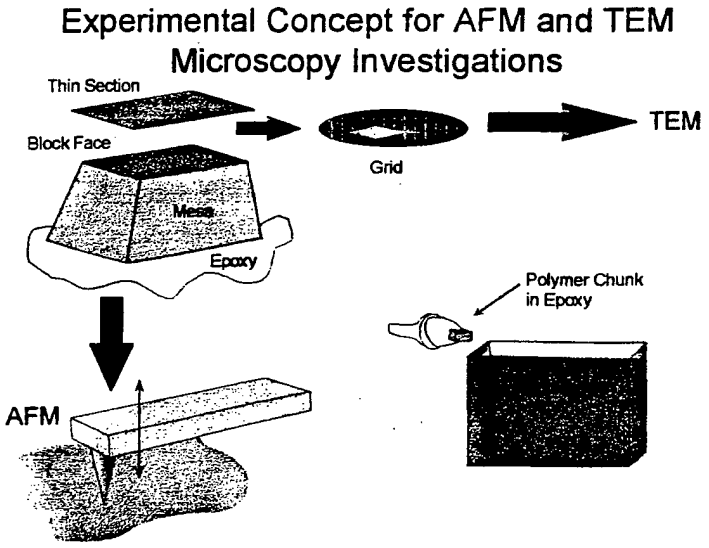

Figure 10-III . Sample preparation for TEM and tapping mode AFM.

Tapping mode AFM was used to probe this fresh block surface. By forcing oscillation of the probe tip cantilever, intermittent contact of the tip with the sample surface was achieved. The tip rastered in the x (fast scan) and y (slow scan) axes. Up to 512 data points/raster can be collected and the probe tip may raster up to 512 times per image allowing for 512 x 512 pixels/image. The two types of data acquisition used to construct accurate topographical information are height imaging and amplitude imaging. Information relating to the distribution of what might be roughly considered "local mechanical modulus," or hard vs. soft regions across the sample surface is collected using phase imaging which is quite appropriate within the context of these block copolymers having hard and soft domains. A crude depiction of AFM operation is provided in Figure 11-III for the purpose of understanding the nature of the images collected in the different modes.

Height: Height data gives accurate information about only the z-axis position of the probe tip over the surface. The change in the z-axis is plotted as a topographical map of the surface.

Amplitude: Amplitude images tend to show edges of surface features well and give accurate information only about features in the x-y directions. The relative amplitude of the cantilever is monitored by a four quadrant photodiode detector. The RMS value of the laser signal on the y-axis on the detector is recorded for each of the 512 segments on a given raster of the probe tip. These values are plotted as an amplitude map of the sample surface. Surface elasticity is correlated to the amount of damping experienced by the cantilever, and is monitored by noting changes in the RMS amplitude signal.

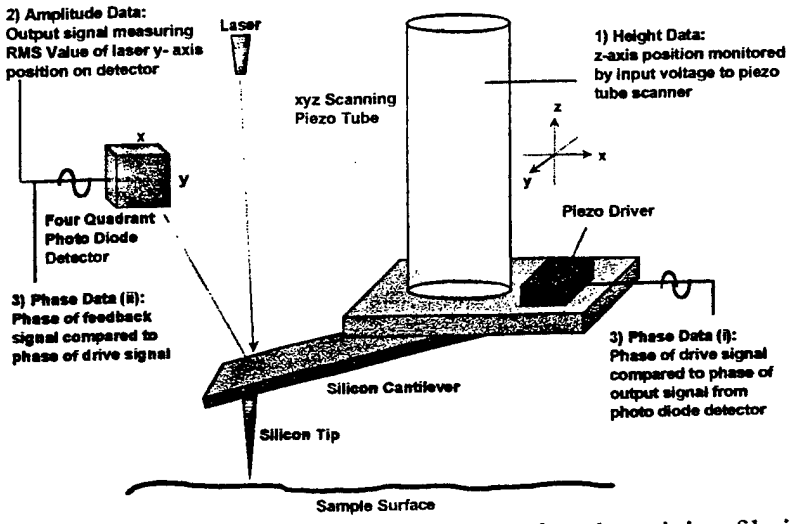

Figure 11-III. AFM probe tip and scanning head showing the origin of height, amplitude and phase data.

Phase: Phase imaging gives information relating to the distribution of relative local elasticity over the sample surface. The phase of the drive signal to the piezo stack is compared to that of the output signal of the laser on the four quadrant photodiode detector as shown in Figure 11-III. The contrast seen in an image is proportional to the extent to which these two signals are out of phase. This concept is similar to that in the science of viscoelasticity which addresses the phase between a driven periodic strain and resultant stress. Thus, the stiffer PS domains are expected to yield a different phase than the elastomeric PIB regions.

Results

AFM. The cutting direction of the diamond knife relative to the AFM images, seen in Figures 12, 13 and 14-III, is from bottom left to top right and knife marks run in this cutting direction. It is conjectured that the specimen has undergone successive compression followed by tearing as the knife passed through the specimen. The

compression marks consist of the striations, or bands, that are seen perpendicular to the cutting direction. This is, of course, to be viewed as an artifact.

The morphology consisting of an array of cylinders was uncovered and is seen with most clarity in the phase image. This morphology is also seen on the amplitude image (Figure 12-III) but with more difficulty, and not at all on the height image (Figure 13-III). Knife marks are distinctive in the height and amplitude images. In the phase image (Figure 14-III), most of the PS cylindrical axes appear to be perpendicular to the cutting direction, although there are some domains of parallel cylinders that appear to be more or less parallel to the surface in this particular field of view. Efficient hexagonal packing of the cylinders is seen upon closer inspection in some regions where the cylinders are perpendicular to the surface. The center-to-center spacings of these cylinders is roughly in the range of tens-of-nanometers. Thus, these materials can indeed be classified as "nanocomposites". There are macrodomains in which the all the cylinders are in the same direction and macrodomain boundaries at which the cylinder direction changes. Here, the word "macrodomain" is used to refer to such a collection of parallel cylinders, whereas the word "domain" was used previously to refer to a single smaller cylinder in the dispersed PS phase.

A very important point to make here is that the natural phase separated morphology of the unmodified BCP has been preserved despite the invasion of this template by an *in situ*-grown, sol-gel-derived silicate phase. This visual evidence lends credence to our previous working "template hypothesis," and lends support to the indirect evidence that was previously cited.

Figure 12-III. Tapping mode AFM *height* image for a $BTMA^+$ form BCPI composite having 6.5% inorganic uptake. Image dimensions are 4 μm x 4 μm.

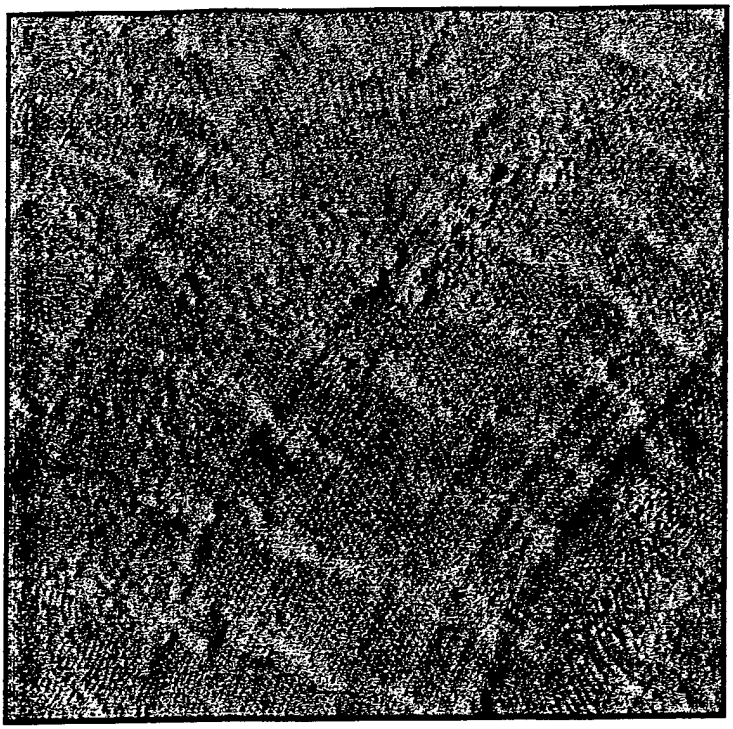

Figure 13-III. Tapping mode *amplitude* image for a $BTMA^+$ form BCPI composite having 6.5% silicate uptake. Image dimensions are 4 μm x 4 μm.

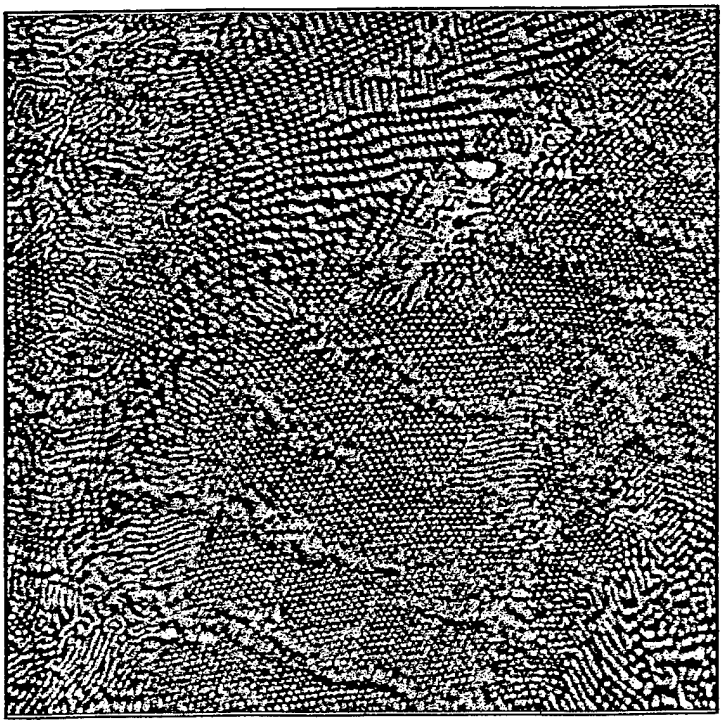

Figure 14-III. Tapping mode *phase* image of $BTMA^+$ form BCPI composite 6.5% uptake. The very distince light regions are cylindrical PS domains. Image dimensions are 4μm x 4 μm.

TEM. First, unstained sections of the BCPI and BCPI/silicate samples were examined. Then, each of the two sections was stained with RuO_4 and then re-examined. Figures 15 and 16-III are images for the stained and unstained composite having 8.5% silicate. Good contrast between the PS and PIB phases is in fact seen regardless of whether the sample was stained. The considerable electron density contrast between the phases is obviously enhanced by the segregation of the silicate component around/in the PS domains while the electron density of the PIB phase maintains the low value of a hydrocarbon. If the silicate phase is indeed structured along these cylinders rather than dispersed homogeneously, then the percent silicate in the PS domains is higher than the bulk average of 8.5%. These TEM micrographs depict a morphology of locally-parallel cylinders that was also seen in the above AFM micrographs. Here, however, the sample is such that the cylinder direction appears to be off-axis relative to the normal to the image. This is seen more clearly on the stained micrograph which also illustrates a macrodomain boundary.

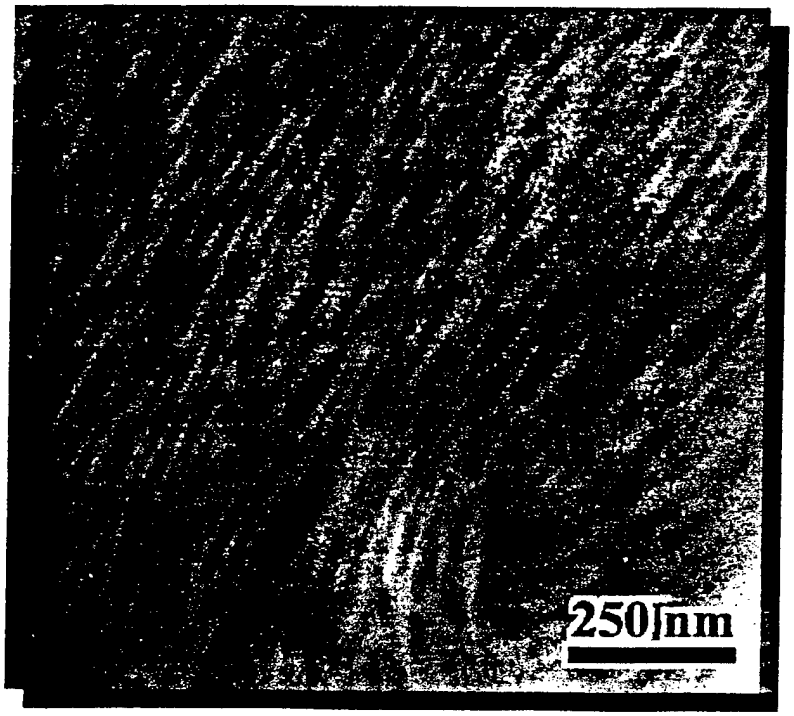

Figure 15-III. TEM micrograph for an *unstained* $BTMA^+$ form BCPI with 8.5% silicate.

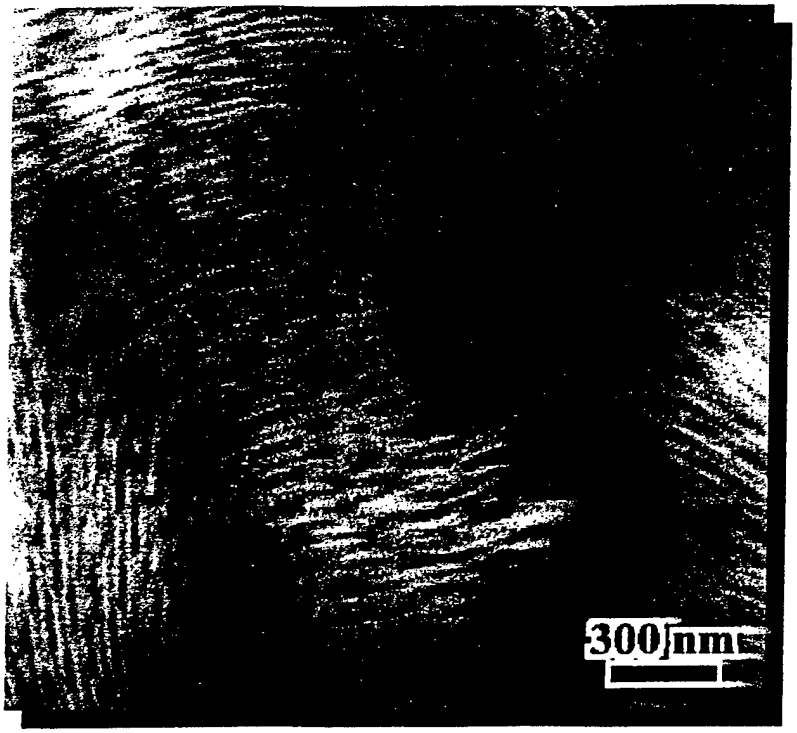

Figure 16-III. TEM micrograph for a $BTMA^+$ form BCPI having 8.5% silicate, but *stained* with RuO_4.

i. Small Angle X-Ray Scattering (SAXS) Investigations of Nanostructure. SAXS experiments were conducted on the $BTMA^+$ form BCPI and BCPI/silicate nanocomposites in collaboration with Dr. Nora Beck Tan at the Army Research Laboratories. These studies were meant to uncover structural information that reinforces/ complements that deriving from our TEM and AFM investigations. In contrast with select area high resolution microscopy, SAXS interrogates structures that are ensemble-averaged over a macroscopic (albeit small) sample in the path of the beam. Structural information is in the form of peaks that lie on scattered x-ray intensity vs. wave vector magnitude curves. The wave vector magnitude, q is equal to $2\pi/d$, where d is the Bragg spacing associated with the given peak that reflects a structural periodicity based on electron density contrast variation. The simple appearance of several strong peaks in the scattering pattern is evidence for extensive *self-assembly*.

On inspecting the SAXS profiles in Figure 17-III, it might seem that the unfilled $BTMA^+$ form BCPI in fact exhibits a lower degree of order than that of either composite based on the multiplicity and definition of peaks. At least superficially, the *in situ* sol-gel process seems to refine the template morphology. On the other hand, the increased order may only be apparent from the standpoint that the increased contrast between the PS and PIB phases simply enhances the peaks rather than being reflective of intrinsic structural refinement. As mentioned earlier, increased electron density around the PS domains is due to incorporation of the silicate component around/in these regions. In the case of the two composites, the peak spacings indicate cylindrical morphology. The peaks in Figure 17-III are clustered in a q region that corresponds to d spacings on the order of tens-of-

nanometers. Thus, this SAXS data is in harmony with the structures observed by means of TEM and AFM.

SAXS experiments are ongoing in cooperation with Dr. Nora Beck Tan at ARL.

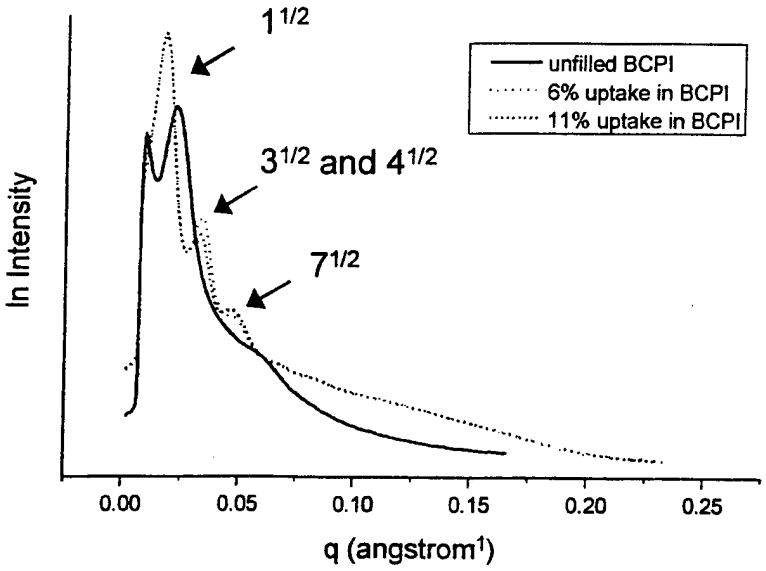

Figure 17-III. SAXS profiles for the $BTMA^+$ form BCPI and BCPI/silicate composites. M_w of the parent BCP is 76,900 with 18 mole % PS of which 16 mole % was sulfonated.

j. ^{23}Na NMR Spectroscopic Investigations

^{23}Na solid state NMR spectra were obtained using a Bruker 200 MHz solid state NMR spectrometer. The series of three spectra shown in Figure 18-III is for a Na^+ form BCPI that has no silicate component. Like experiments involving silicate-filled systems are planned. The mole % PS is 18% of which 12.8% is sulfonated. The 'as cast' spectrum refers to a BCPI sample that was prepared by film casting and allowed to sit on the bench top as exposed to ambient air and humidity. The 'dry' spectrum refers to an as cast film, but placed in a vacuum oven at 100°C for 4d, and subsequently stored in a desiccator. The spectrum labeled 'hydrated' was obtained from a BCPI film that was subjected to boiling water and then remained in contact with water in a room temperature storage condition.

We attribute he sharp resonance at *ca.* 10 ppm to isolated sodium sulfonate groups while the broad peak centered about –20 ppm for the 'as cast' and dry samples is attributed to clustered $-SO_3^- Na^+$ ion pairs, as discussed by Cooper *et al.*[27] and later by Moore *et al.* with regard to sulfonated polystyrene ionomers[28] The small peak occurring at about 0 ppm is attributed to hydrated, presumably dissociated Na^+ ions . The 'hydrated' BCPI spectrum shows that almost the entire population of Na^+ ions is in fact characterized by hydration, a condition that was discussed by Mauritz and Komoroski with regard to the Na^+ form of Nafion sulfonate membranes.[29]

In addition to other pertinent results above, this experiment demonstrates that these materials can incorporate water, which is desirable within the context of their application as CWA resistant barriers that transport water.

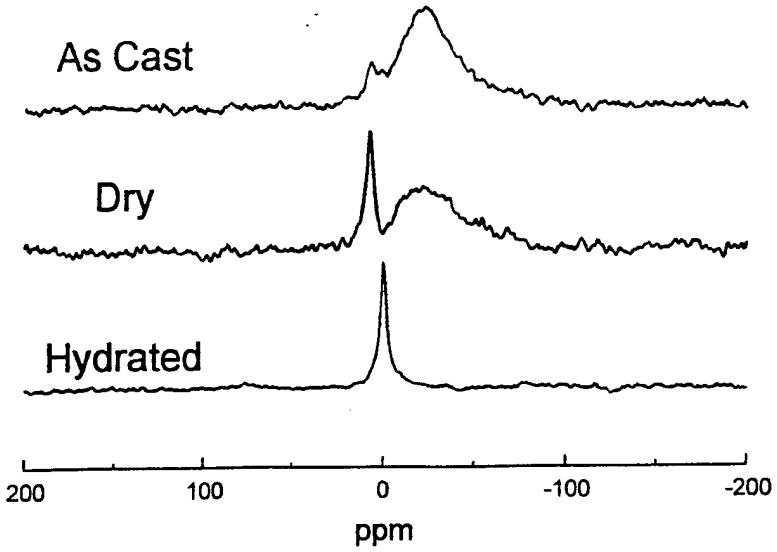

Figure 18-III. ^{23}Na NMR spectra for a Na^+ form BCPI. The same sample was exposed to the different indicated conditions.

IV. EXTERNAL COLLABORATION

A. DR. NORA BECK TAN, ARMY RESEARCH LABORATORIES (ARL), ABERDEEN PROVING GROUND

We have established a substantive research collaboration with Dr. Nora Beck Tan at ARL. She has conducted small angle X-ray scattering (SAXS) investigations on the $BTMA^+$ form BCPI and BCPI/silicate composites to aid in the elucidation of their nanostructures. These studies were meant to uncover structural information that reinforces, or complements that deriving from our TEM and AFM investigations and the results are discussed earlier in this report. Dr. Beck Tan also visited the University of Southern Mississippi to discuss these results with our research team as well give a presentation on her research activities at ARL. It is planned that this collaboration will continue and that a student from the Mauritz research group will spend time at ARL so as to assist Dr. Beck Tan in the SAXS experiments.

B. NATICK RESEARCH, DEVELOPMENT AND ENGINEERING CENTER (NRDEC)

Mauritz and Storey traveled to NRDEC Feb 10 to meet with Dr. Donald Rivin at the U.S. Army Soldier Systems Command to become aware of important issues regarding our materials in relation to the ARO mission in the area of CWA-resistant materials. We also presented the results of our research along with other ARO contractees in a series of seminars and thereby became aware of other research activities in this arena.

THIS

PAGE

IS

MISSING

IN

ORIGINAL

DOCUMENT

41

VI. PUBLICATIONS RESULTING FROM ARO FUNDING

1. Reuschle, D.A.; Mountz, D.A; Brister, L.B.; Curry, C.L.; Shoemake, K.A.; Storey, R.F.; Mauritz, K.A. "Thermal Analysis of Poly(Styrene-*co*-Isobutylene-*co*-Styrene) Block Copolymers and Block Copolymer Ionomers" *ACS Div. Polym. Chem., Polym. Preprs.* **1998**, *39*(1), 381.

2. Mountz, D.A.; Reuschle, D.A.; Brister, L.B.; Storey, R.F.; Mauritz, K.A. "Swelling of, and Sol-Gel Reactions within Poly(Styrene-*b*-Isobutylene-*b*-Styrene) Ionomers" *ACS Div. Polym. Chem., Polym. Preprs.* **1998**, *39*(1), *39*(1), 383.

3. Mauritz, K.A.; Mountz, D.A.; Reuschle, D.A.; Storey, R.F. "Organic/Inorganic Nanocomposites as Potential Fuel Cell Membranes," *Proceedings of the DOD Workshop on Advanced Fuel Cell Membranes*, Las Vegas, Clemson U. In press.

4. Storey, R.F.; Brister, L.B. "Developments Towards Superior Poly(styrene-b-isobutylene-b-styrene) Block Copolymers Synthesized by Living Cationic Polymerization," in preparation.

5. Storey, R.F.; Shoemake, K.A. "Multi-Arm Star-Branched Polyisobutylene Ionomers," *Polym. Bull.* **1997**, *39*, 393.

6. Storey, R.F.; Shoemake, K.A. "Effect of Reaction Conditions on Synthesis and Properties of Multi-Arm Star-Branched Polyisobutylene," *J. Polym. Sci.: Part A: Polym. Chem.* **1998**, *36*, 471.

7. Storey, R.F.; Baugh, D.; Choate, K.R. "Poly(styrene-*b*-isobutylene-*b*-styrene) Block Copolymers Produced by Living Cationic Polymerization. I. Compositional Analysis," *Polymer*, accepted.

8. Storey, R.F.; Baugh, D. "Poly(styrene-*b*-isobutylene-*b*-styrene) Block Copolymers Produced by Living Cationic Polymerization III: Dynamic Mechanical and Tensile Properties," in preparation.

9. Storey, R.F.; Baugh, D. "Poly(styrene-*b*-isobutylene-*b*-styrene) Block Copolymers Produced by Living Cationic Polymerization II: Morphology of Block Copolymers and Ionomers Therefrom by Small-Angle X-ray Scattering and Transmission Electron Microscopy," *Polymer*, submitted.

10. Storey, R.F.; Brister, L.B "On the Use of Methylcyclohexane as a Cosolvent for the Living Cationic Polymerization of Poly(styrene-b-isobutylene-b-styrene) Block Copolymers, *ACS Div. Polym. Chem., Polym. Preprs.* **1997**, *38*(2), 287.

VII. 1998 STUDENT THESES AND DISSERTATIONS RESULTING FROM ARO FUNDING

None in 1998.

VIII. SCIENTIFIC PERSONNEL SUPPORTED IN WHOLE OR IN PART BY ARO FUNDS

1. Kenneth A. Mauritz, Professor, Department of Polymer Science. P.I.
2. Robson F. Storey, Professor, Department of Polymer Science. P.I.
3. David A. Mountz, Polymer Science Graduate Student. Started June 1997.
4. David A. Reuschle, Polymer Science Graduate Student. Partial support.
5. L. Brian Brister, Polymer Science Graduate Student. Partial support.
6. Christopher Curry, Polymer Science Graduate Student. Started June 1996.

IX. LITERATURE REFERENCES

(1) Deng, Q.; Moore, R.B.; Mauritz, K.A. *Chem. Mater.* **1995**, *7*, 2259.
(2) Gummaraju, R.V.; Mauritz, K.A. *J. Polym. Sci.: Part B.: Polym. Phys.* **1996**, *34*, 2383.
(3) Greso, A. J.; Moore, R.B.; Cable, K.M.; Jarrett, W.L.; Mauritz, K.A. *Polymer* **1997**, *38* (6), 1345.
(4) Juangvanich, N.; Mauritz, K.A. "Polyethersulfone/(Silicon Oxide) Hybrid Materials via in Situ Sol-Gel Reactions for Tetraalkoxysilanes," *J. Appl. Polym. Sci.*, in press.
(5) Cunningham, R.E.; Williams, R.J. *Diffusion in Gases and Porous Media* Plenum: New York, 1980.
(6) Kaszas, G.; Puskas, J. E.; Kennedy, J. P.; Hager, W. G. *J. Polym. Sci., Polym. Chem. Ed.* **1991**, *29*, 427.
(7) Gyor, M.; Fodor, Z.; Wang, H.-C.; Faust, R. *J.M.S.-Pure Appl. Chem.* **1994**, *A31*(12), 2055.
(8) Storey, R.F.; Donnalley, A.B.; Maggio, T.L. *Macromolecules* **1998**, *31*, 1523.
(9) Storey, R.F.; Choate, K.R. *Macromolecules* **1997**, *30*, 4799.
(10) Hen, B-H; Boudjouk, P. *Organometal.* **1983**, *2*, 769.
(11) Marcineic, B.; Urbaniak, W. *J. Mol. Catal.* **1983**, *18*, 49.
(12) Chalk, A.; Harod, J.F. *J. Am. Chem. Soc.* **1967**, *89*, 1640.

(13) Marciniec, B. *Comprehensive Handbook on Hydrosilylation*. Pergamon Press: New York, 1992, pp. 37-38.
(14) Kaddami, H.; Gérard, J.F., Pascault, J.P.; Lam, T.M. *Proceedings of the First European Workshop on Hybrid Organic-Inorganic Materials*, Paris, 1993, p.9.
(15) Storey, R.; Chisholm, B.; Lee, Y. *Polymer* **1993**, *34*, 4330.
(16) Bates, F. *Science* **1991**, *251*, 898.
(17) Weiss, R.; Sen, A.; Willis, C.; and Pottick, L. *Polymer* **1991**, *32*, 1867.
(18) Storey, R.F.; Baugh, D.; Choate, K.R. "Poly(styrene-*b*-isobutylene-*b*-styrene) Block Copolymers Produced by Living Cationic Polymerization. I. Compositional Analysis," *Polymer*, accepted.
(19) Mountz, D.; Reuschle, D.; Brister, B.; Storey, R.; and Mauritz, K. *ACS Div. Polym. Chem., Polym. Preprs.* **1998**, *39(1)*, 383.
(20) Zeng, Z.; Mauritz, K. *Macromolecules* **1992**, *25*, 2369.
(21) Reuschle, D.; Mountz, D.; Brister, B.; Storey, R.; and Mauritz, K *ACS Div. Polym. Chem., Polym. Preprs.* **1998**, *39(1)*, 381.
(22) Plazek, D.; Chay, I.; Ngai, K.; Roland, C. *Macromolecules* **1995**, *28*, 6432.
(23) Storey, R.F.; Baugh, D. "Poly(styrene-*b*-isobutylene-*b*-styrene) Block Copolymers Produced by Living Cationic Polymerization III: Dynamic Mechanical and Tensile Properties," in preparation.
(24) Eisenberg, A.; Hird, B.; Moore, R. *Macromolecules* **1990**, *23*, 4098.
(25) a. Maxwell, J.C. *A Treatise on Electricity and Magnetism*, 2nd Ed.; Clarendon: Oxford, 1881; p 398.
b. Wagner, K.W. *Arch. Electrotech. (Berlin)* **1914**, *2*, 371.
c. Sillars, R.W. *J. Inst. Electr. Eng.* [1889-1940] **1937**, *80*, 378.
d. Mauritz, K.A.; Fu, R.M. *Macromolecules*, **1988**, *21*, 1324.
(26) Mountz, D.A.; Reuschle, D.A.; Mauritz, K.A. *ACS Div. Polym. Chem., Polym. Preprs.* **1998**, *39*(1), 383.
(27) a. O'Connell, E.M.; Root, T.W.; Cooper, S.L. *Macromolecules* **1994**,*27*, 5803.
b. O'Connell, E.M.; Root, T.W.; Cooper, S.L. *Macromolecules* **1995**, *28*, 3995.
c. O'Connell, E.M.; Root, T.W.; Cooper, S.L. *Macromolecules* **1995**, *28*, 4000.
d. O'Connell, E.M.; Peiffer, D.G.; Root, T.W.; Cooper, S.L. *Macromolecules* **1996**, *29*, 2124.
(28) Gummaraju, R.V.; Moore, R.B. *ACS Div. Polym. Chem., Polym. Preprs.* **1998**, 39(1), pg. 387.
(29) Komoroski, R.A.; Mauritz, K.A. in "Perfluorinated Ionomer Membranes," Eisenberg, A.; Yeager, H.L., Eds., *Am. Chem. Soc. Symp. Ser.* **1982**, *180*, Ch. 7.